STRUCTURAL ANALYSIS OF INTERIOR LAYERED DEPOSITS IN NORTH AND SOUTH COPRATES CHASMA, MARS

Heather Racher, Hons. B.Sc.

Master of Science in Earth Science

Submitted in partial fulfillment of the requirements for the degree of

Master of Science

Faculty of Mathematics and Science, Brock University,

St. Catharines, Ontario, Canada

ABSTRACT

Interior layered deposits within an embayment in the northern as well as near the southern wall of Coprates Chasma in the Valles Marineris, Mars are studied using HRSC, CTX, HiRISE and CRISM data. In the northern embayment, layered deposits outcrop in three separate locations (a western deposit, a central deposit and an eastern deposit). The central layered deposit in the north has a stratigraphic thickness of 2 km. The western layered deposit abuts against the chasma wall appearing to have a relatively un-eroded depositional surface. The eastern deposit is near a landslide scar which appears to have exposed basement layering showing downward displacement. This northern embayment is suggested to have been an ancestral basin.

The triangular edged deposit near the southern wall of Coprates Chasma has an elongated mound protruding from the central edge and is suggested to be the outer limits of a fault block which is back rotated 6° south. The rotation may be the result of the Valles Marineris opening.

TABLE OF CONTENTS

LIST OF TABLES

LIST OF FIGURES

CHAPTER 1 – INTRODUCTION AND OVERVIEW

The term ILD is used to describe layering deposited in sequence to form an interior layered deposit. These layered deposits (ILDs) are found within the chasmata of Valles Marineris on Mars. Generally, these deposits unconformably overlie canyon floors or walls (Komatsu *et al.*, 2004) and the layering of varying thicknesses ranges from tens of meters to hundreds of meters thick. The origin and mechanism of ILD formation is uncertain and several hypotheses have been proposed, including lacustrine (Nedell *et al.*, 1987), aeolian (Peterson, 1981), spring deposits (Rossi *et al.*, 2008), pyroclastic volcanism in subaerial (Hynek *et al.*, 2003; Chapman, 2002; Lucchitta, 1987, 1990) or in subglacial (Nedell *et al.*, 1987; Chapman and Tanaka, 2001; Komatsu *et al.*, 2004) environments. These processes imply the troughs within which the ILDs formed are older than these layered deposits. It has also been suggested that ILDs are ancient deposits buried beneath the material which forms the walls of troughs (Malin and Edgett, 2000; Catling *et al.*, 2006). The diversity of ILD characteristics implies that several mechanisms were involved in their formation. These deposits provide insight into the depositional environment in which they formed and also the post depositional deformation. The purpose of this study is to examine two locations of interior layered deposits and identify the possible formation mechanisms in Coprates Chasma within Valles Marineris.

High Resolution Stereo Camera (HRSC) data; the image and corresponding DEM from orbit 2039 was provided by Ernst Hauber from the Institute of Planetary Research, German Aerospace Center, (DLR) in Berlin, Germany. The HRSC image covers a section of Coprates Chasma and the corresponding Digital Elevation Model (DEM) with

a grid spacing of 50 m was used as the base of investigation of the project (Fig. 1-1). Also used were higher resolution images; context images (CTX: 6 m per pixel) and High Resolution Imaging Science Experiment (HiRISE: 25 m per pixel) images. Orion software used for attitude measurements was provided by Bob Stesky at Pangaea Scientific in Brockville, Ontario. Hyperspectral data obtained for the CRISM analysis to determine the mineralogical content of the central northern layered deposit in Coprates Chasma was done by Patrick McGuire at the Institute of Planetary Research, German Aerospace Center (DLR), Berlin, Germany.

Figure 1-1. The HRSC image from orbital path 2039 covers the extent of the study area; north and south Coprates Chasma. The image scale is 250 km by 64 km. The red box indicates the north area of interest and the yellow box indicates the southern extent. (Jaumann *et al.*, 2007)

This thesis is presented as a series of chapters, two of which are intended as stand-alone publications.

Chapter 2 provides a general background on Mars with a focus on the geological timescale with respect to the timing of major events. The formation of the Tharsis Bulge, Valles Marineris and Coprates Chasma are outlined as part of a larger geological history. The models and theories of formation mechanisms of other interior layered deposits are reviewed.

Chapter 3 and 4 are intended as stand-alone publications and for that reason, there is some duplication.

Chapter 3, entitled *Structural Analysis of Interior Layered Deposits in Northern Coprates Chasma on Mars* is published in a special HRSC volume of EPSL (Earth and Planetary Science Letters). The paper focuses on the northern study area and investigates three layered deposits with attitude measurements and CRISM analysis to provide a general hypothesis of the formation of these deposits but also, an idea of the overall formation of this part of the chasma. An embayment within Coprates Chasma is proposed to be a small ancestral basin likely linked during the opening of the Valles Marineris.

Chapter 4 is entitled *Structural Analysis of an Interior Layered Deposit in Southern Coprates Chasma on Mars.* The southern ILD and surrounding location is analyzed with attitude measurements. CRISM data is not currently available for this investigation and general interpretations from imagery were acquired. The southern area is separated into two deposits; the main mound and the elongated mound. Layered deposits are found along the triangular edges and on the top of the main mound. It is

proposed the main mound is a fault block which has been back rotated. The adjacent elongated mound is suggested to have once been part of the larger fault block and pulled back during the rotation.

Chapter 5 discusses the overall conclusions and similarities present between the two locations and deposits. Similarities are identified to provide an interpretation of the formation of Coprates Chasma as whole enclosed sub basin and later linked to the Valles Marineris. ILD formation mechanisms are narrowed yet a single mechanism could not be deemed responsible for the deposits seen within the chasma.

REFERENCES

Catling, D.C., S.E. Wood, C. Leovy, D.R. Montgomery, H.M. Greenberg, C.R. Glein, J.M. Moore. 2006. Light-toned layered deposits in Juventae Chasma, Mars. *Icarus, 181*: 26-51.

Chapman, M.G. 2002. Layered, massive, and thin sediments on Mars: Possible Late Noachian to Late Amazonian tephra? In: Smellie, J.L. and M.G. Chapman, (eds). Volcano-Ice Interactions on Earth and Mars. *Geological Society, London, Special Publications, 202*: 273-203.

Chapman, M.G. and K. Tanaka. 2001. Interior trough deposits on Mars: Subice volcanoes? *Journal of Geophysical Research, 106(E5)*: 10,087-10,100.

Hynek, B.M., R. Phillips, and R. Arvidson. 2003. Explosive volcanism in the Tharsis region: Global evidence in the Martian record. *Journal of Geophysical Research, 108(E9), 5111*, doi:10.1029/2003JE002062.

Jaumann, R., G. Neukum, T. Behnke, T.C. Duxbury, K. Eichentopf, J. Flohrer, S.V. Gasselt, B. Giese, K. Gwinner, E. Hauber, H. Hoffmann, A. Hoffmeister, U. Köhler, K-D Matz, T.B. McCord, V. Mertens, J. Oberst, R. Pischel, D. Reiss, E. Ress, T. Roatsch, P. Saiger, F. Scholten, G. Schwarz, K. Stephan, M. Wählisch, and the HRSC Co-Investigator Team. 2007. The high-resolution stereo camera

(HRSC) experiment on Mars Express: Instrument aspects and experiment conduct from interplanetary cruise through the nominal mission. *Planetary Space Science, 55*: 928-952.

Komatsu, G., G.G. Ori, P. Ciarcelluti, and Y.D. Litasov. 2004. Interior layered deposits of Valles Marineris, Mars: analogous subice volcanism related to Baikal Rifting, Southern Siberia. *Planetary Space Science, 52*: 167-187.

Lucchitta, B.K. 1990. Young Volcanic Deposits in Valles Marineris, Mars? *Icarus, 86*: 476-509.

Lucchitta, B.K. 1987. Recent mafic volcanism on Mars. *Science, 235*: 565-567.

Malin, M.C., and K.S. Edgett. 2000. Sedimentary rocks of early Mars. *Science, 290*: 927-1938.

Nedell, S., S. Squyres, and D. Andersen. 1987. Origin and evolution of the layered deposits in the Valles Marineris, Mars. *Icarus, 70*, 409-441.

Peterson, C. 1981. A secondary origin for the Central Plateau of Hebes Chasma. Proc. *12th Lunar and Planetary Science Convention*, Part B, Pergamon Press: New York, 1459-1471.

Rossi, A.P., G. Neukum, M. Pondrelli, S. Van Gasselt, T. Zegers, E. Hauber, A. Chicarro, and B. Foing. 2008. Large-scale spring deposits on Mars? *Journal of Geophysical Research, 113(EO), 8016,* doi:10.1029/2007JE003062.

CHAPTER 2 – MARS BACKGROUND

Geological Time Scale

The geological timescale provides approximate ages for the units and structures observed on Mars. The dating is based on the density and size of craters visible on the surface. Crater counting is a method for identifying approximate ages for geological units and structures on Mars. The geologic history is divided into three Epochs: the oldest, Noachian, the Hesperian and the youngest, Amazonian (Fig. 2-1). The units are named for specific geological regions. The Noachian Epoch is named for the Noachis Terra, Hesperian Epoch for the Hesperia Planum and the Amazonian Epoch for the Amazonis Planitia (Solomon *et al.*, 2005). The Noachian Epoch began as early as 4.5 billion years ago with the planetary crustal formation and during the first billion years, Mars was the most active with widespread volcanism including the formation of the Tharsis Bulge. Head *et al.* (2001) suggested that the peak of fluvial activity would have occurred during this time with the evidence of Noachian aged valley networks. Crater impacts of the Noachian Epoch are large in diameter and densely concentrated on the surface. The Hesperian Epoch began 3.5 billion years ago and ended 1.8 billion years ago (Head *et al.*, 2001). Volcanism appears to be less extensive and more concentrated in regional terrains such as the Olympus Mons within the Tharsis Bulge. The rift valley system, Valles Marineris was formed in the later Hesperian. Crater impacts were less frequent with ranging diameters and most geological activity began to taper off near the end of the Epoch. The Amazonian Epoch is the youngest unit, beginning 1.8 billion years ago to present day (Head *et al.*, 2001) and minimal geological activity is recorded during this time frame. Coprates Chasma was formed by the early Amazonian. Aeolian

processes are the only recently recorded geological activity on Mars. Craters associated with the Amazonian Epoch are uncommon and relatively small in diameter.

Figure 2-1. The crater density scale separates each geological unit by age. The Noachian began 4.5 billion years ago and until 3.5 billion years ago. The Hesperian started 3.5 billion years ago until 1.8 billion years ago. The Amazonian began 1.8 billion years ago and continues to present day. (Gangale, 2007)

Geological Setting

Tharsis Bulge

The Tharsis Bulge covers approximately 10% of the planet's surface which is equivalent to the size of North America's land surface (Bridges, 2004) and is a volcanic system on the Mars equator, within the southern highlands (Fig. 2-2). Valles Marineris is situated within the eastern end of the Tharsis Bulge. Volcanism affected at least half of the Mars surface, and may have continued as recently as 25 million years ago (Mangold *et al.*, 2000). The Tharsis Bulge has the highest relief on Mars rising to a height of 10 km and was formed in the Noachian Epoch through to the Late Hesperian Epoch (Mangold *et al.*, 2000). The formation of the Tharsis Bulge occurred in three separate volcanic stages. The first stage of formation occurred as a combination of volcanism and resulting isostatic competency (Mangold *et al.*, 2000). Volcanism loaded the crust to a critical point and the crust was not able to support the added weight of the Tharsis Bulge. The added weight caused the surface to fracture and with further tectonism widened the fractures to eventually create drainage valleys during the late Noachian (Mangold *et al.*,

2000). The second stage continued with more volcanism and the loss of isostatic equilibrium (Mangold *et al.*, 2000). Continued pressure of the Tharsis Bulge created a very large load and the crust failed producing radial fractures around the Tharsis Bulge (Peulvast *et al.*, 1994). The third stage continued with more volcanism, the crust reached failure, and the youngest volcanoes on the Tharsis Bulge began to form (Mangold *et al.*, 2000). The Tharsis Bulge has 12 large shield volcanoes which formed through centralized magma flow. Olympus Mons, shaped by volcanism associated with a mantle plume during the Noachian when the planet was still undergoing active cooling (Bridges, 2004) is the largest volcano on Mars and within the solar system (Fig. 2-2).

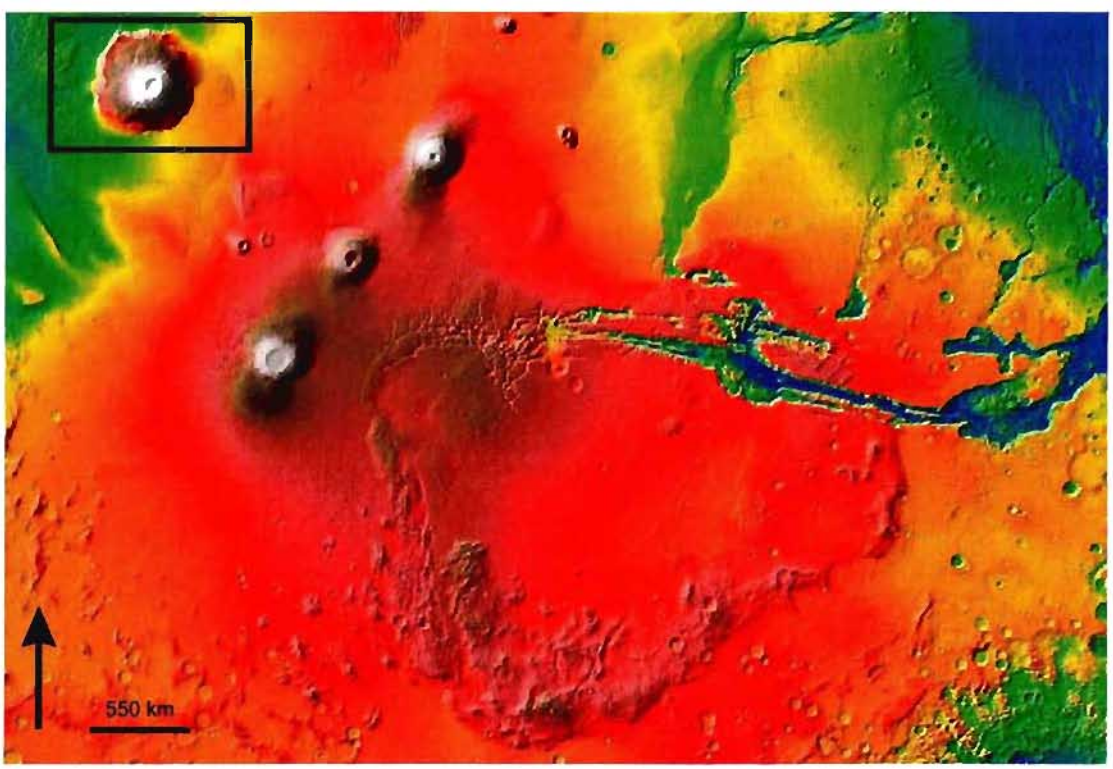

Figure 2-2. The elevation map shows the extent of the Tharsis Bulge as a large red mass with an elevation greater than 3 km. The Valles Marineris is the long canyon in blue with an elevation less than -3 km to the right of the Tharsis Bulge. The Olympus Mons is indicated in the black box in the north west corner. (NASA, 2007)

Valles Marineris

The Valles Marineris is Latin for Mariner Valleys and the valley is named for the Mariner 9 orbiter that imaged the system in 1971 to 1972 (Shultz *et al.*, 2001). The Valles Marineris is considered to be a large rift valley (Lucchitta *et al.*, 1994), 4000 km long and 10 km deep. The rift valley is located south of the equator in the southern highlands and to the east of the Tharsis Bulge. The Valles Marineris consists of numerous linked sub basins producing the current configuration. The chasmata of Valles Marineris were likely formed during a two stage process (Lucchitta *et al.*, 1994; Schultz, 1998). Ancestral basins which are isolated depressions with irregular outlines were proposed to have formed prior to the opening of the Valles Marineris during rift-like faulting (Lucchitta and Bertolini, 1990; Lucchitta *et al.*, 1994). Lucchitta *et al.* (1994) suggests that Hebes, south Ophir, south Candor and potentially south Melas Chasma were sites of ancestral basins. It is noted, much of Coprates Chasma, north Melas and Ius may have formed during the later faulting episodes (Lucchitta *et al.*, 1994). Closed depressions appear to have no lateral removal of material and require a downward displacement, a collapse of material into a pre-existing void (Shultz, 1997). Whereas the chasmata that formed later with tectonism have rectangular troughs consistent with the mechanism yet; faulting cannot account for all the irregular outlines of the basins (Shultz, 1997). Faulting resulting from the opening of the Valles Marineris (Schultz, 1998) connected surrounding basins and formed the current rift valley configuration.

Grabens, depressions bounded by faults, are observed in the Valles Marineris and are the largest recorded on Mars (Shultz *et al.*, 2001). The graben forming faults cut across older troughs to further widen the walls. The grabens broke through walls of

troughs and created new, larger ones. The ILDs within the depressions are displaced and tilted from the faults which were formed from the presence of grabens (Shultz *et al.*, 2001). The erosional and depositional mechanisms within Valles Marineris are widely debated and theories of possible fluvial activity are not thoroughly investigated. The rift system is comprised of different types of troughs and walls. The troughs, narrow depressions, are observed as either scalloped troughs and pit crater chains or straight well aligned troughs (Peulvast *et al.*, 1994). There are also three categories of walls that are commonly associated with specific types of troughs. The first wall type is spur and gully found along the straight well aligned troughs (Peulvast *et al.*, 1994). Gullies are associated with vertical erosion caused by flow from the surrounding plateau, continuing the widening of the Valles Marineris (Peulvast *et al.*, 1994). The second wall structure is dissected by tributary canyons. This wall structure is similar to the gully formation however; this structure is found on larger scales. The third type of wall is formed from the remnants of landslides and has curved or straight recesses in the canyon walls (Peulvast *et al.*, 1994). ILDs are documented to unconformably overlie the Valles Marineris walls and floors (Lucchitta, 1990).

Coprates Chasma

Coprates Chasma is a one of the many chasmata of the Valles Marineris. It is approximately 100 km wide and 8 km deep (Fig. 2-3). Numerous ILDs are found within the chasma floor and within the surrounding wall rock. Hebes, south Ophir, south Candor and south Melas Chasma were possible sites of ancestral basins as suggested by Lucchitta *et al.* (1994). Lucchitta *et al.* (1994) also proposed much of Coprates; north

Melas and Ius may have formed during the later faulting episodes. The trough and graben geology best describes the structure of Coprates Chasma. The interpretation of Coprates Chasma occupying a graben is a common accepted view of the geology within the area (Lucchitta *et al.*, 1994). The formation of Coprates Chasma by keystone collapse of locally elevated topography is not supported by available topographic data. However, trough and volcano - tectonic activity in the Tharsis region is considered to be a likely explanation for the trough forming stresses (Lucchitta *et al.*, 1994).

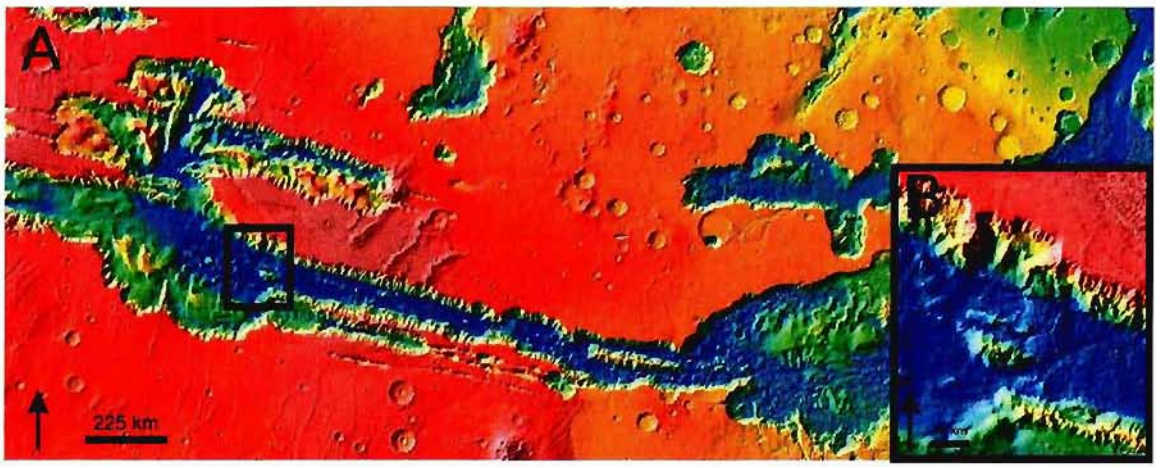

Figure 2-3. Inset A: The elevation map shows the location of western end of Coprates Chasma (black box) with respect to the Valles Marineris. Inset B: The zoomed in view of the western end seen in the black box of inset A. (NASA, 2007)

Interior Layered Deposits

Interior layered deposits (ILDs) occur throughout the chasmata of the Valles Marineris. The layered deposits account for approximately 17% of the total area of Valles Marineris (Lucchitta *et al.*, 1994). The origin and mechanism of ILD formation is unknown. Models of ILD formation are based on the investigation of morphological and stratigraphic characteristics in different depositional environments. Several hypotheses

are proposed, including lacustrine (Nedell *et al.*, 1987), aeolian (Peterson, 1981), pyroclastic volcanism in subaerial (Hynek *et al.*, 2003; Chapman, 2002; Lucchitta, 1987, 1990) or in subglacial (Nedell *et al.*, 1987; Chapman and Tanaka, 2001; Komatsu *et al.*, 2004) environments. Komatsu *et al.* (2004) suggested past stagnant bodies of water with either viscous material or debris settling laterally may account for ILD formations in closed basin settings. The topography surrounding volcanic regions can be comprised of layered deposits which are possibly formed from the debris of successive volcanic events (Hynek *et al.*, 2003). Komatsu and Litasov (2002) suggested centralized vents within subglacial terrains are capped with near horizontal layered deposits above the icy substrate. More recently it has been suggested that ILDs formed as spring deposits (Rossi *et al.*, 2008) and these deposits are indicators of fluvial activity (Clarke and Bourke, 2009). Spring deposits are found in a wide range of scales which Clarke and Bourke (2009) suggested these deposits are unconformable to disconformable capped units from the resulting subsurface characteristics and conditions. All of these processes imply the troughs within which the ILDs formed were created prior to the formation of these ILDs. Alternatively, Malin and Edgett (2000) and Catling *et al.* (2006) suggest ILDs are ancient deposits buried beneath the material which form the walls of troughs. The diversity of ILD characteristics implies that several mechanisms were involved in their formation and can provide an interpretation into past geological conditions.

Mineralogical Data

Mineralogical data from the CRISM analysis suggest water as a mechanism of formation or alteration of ILDs with the presence of sulfates. Mineralogical data suggest

fluvial activity is consistent with the detection of sulfate concentrations (Gendrin *et al.*, 2005; Mangold *et al.*, 2007a, b). Sulfates contain the sulfate anion SO_4^{2-} and form in settings with slow evaporation rates. Milliken *et al.* (2008) suggested that the CRISM data revealed the presence of opaline silica and are associated with sulfate locations on plateau tops surrounding the Valles Marineris troughs. Silicates also contain large quantities of oxygen ions. Chojnacki and Hynek (2008) provide an interpretation of water-altered minerals within Valles Marineris and propose no single formation mechanism is accountable for the available CRISM data. Monohydrated kieserite which is resistant to desiccation often occurs on steeper slopes and this may present limitations on the equatorial distribution of ice during past high obliquity episodes (Vaniman and Chipera, 2006). Chojnacki and Hynek (2008) propose that polyhydrated sulfates often form benches, knobs or hummocky terrain. Kieserite and polyhydrated sulfates are commonly associated with light toned layered deposits. The most probable reason for this difference is the erosional resistance between mono and polyhydrated sulfates (Chojnacki and Hynek, 2008). ILDs within Valles Marineris indicate a diverse sulfate sequence and a variety of hydration process to explain the presence of both mono and polyhydrated sulfates.

REFERENCES

Bridges, John. 2004. Martian Meteorites. [Online]. *National History Museum.* http://www.nhm.ac.uk. October 13, 2007.

Catling, D.C., S.E. Wood, C. Leovy, D.R. Montgomery, H.M. Greenberg, C.R. Glein, J.M. Moore. 2006. Light-toned layered deposits in Juventae Chasma, Mars. *Icarus, 181*: 26-51.

Chapman, M.G. 2002. Layered, massive, and thin sediments on Mars: Possible Late Noachian to Late Amazonian tephra? In: Smellie, J.L. and M.G. Chapman, (eds). Volcano-Ice Interactions on Earth and Mars. *Geological Society, London, Special Publications, 202*: 273-203.

Chapman, M.G. and K. Tanaka. 2001. Interior trough deposits on Mars: Subice volcanoes? *Journal of Geophysical Research, 106(E5)*: 10,087-10,100.

Chojnacki, M. and B. Hynek. 2008. The geological context of water-altered minerals in Valles Marineris, Mars. *Journal of Geophysical Research, 113*: E12005, doi:10.1029/2007JE003070.

Clarke, J., and M. Bourke. 2009. Recognition criteria of spring deposits on Mars at all scales: evidence from the Dalhousie Springs analog (Australia). *40th Lunar and*

Planetary Science Convention, Abstract #1102.

European Space Agency (ESA). 2009. Olympus Mons - the caldera in close-up. [Online]. *Mars Express*. http://www.esa.int/SPECIALS/Mars_Express/SEM9BA1PGQD_1.html. October 25, 2007.

Fueten, F., R. Stesky, P. MacKinnon, E. Hauber, T. Zegers, K. Gwinner, F. Scholten, and G. Neukum. 2008. Stratigraphy and structure of interior layered deposits in west Candor Chasma, Mars, from High Resolution Stereo Camera (HRSC) stereo imagery and derived elevations. *Journal of Geophysical Research, 113*: E10008, doi:10.1029/2007JE003053.

Gangale, Thomas. 2007. Geological Timescales on Earth, Mars and the Moon. [Online]. http://pweb.jps.net/~tgangale/mars/mst/GeologicTimeScales.htm. October 25, 2007.

Gendrin, A., N. Mangold, J. Bibring, Y. Langevin, B. Gondet, F. Poulet, G. Bonello, C. Quantin, J. Mustard, R. Arvidson, and S. LeMouélic. 2005. Sulfates in Martian layered terrains: The OMEGA/Mars Express view. *Science, 307*: 1587-1591.

Hanmer, Simon. 2002. Mars: What we really see in a telescope. [Online]. *Ottawa Center – R.A.S.C.* http://www.ottawa.rasc.ca. October 13, 2007.

Hauber, E., K. Gwinner, A. Gendrin, F. Fueten, R. Stesky, S. Pelkey, H. Wulf, D. Reiss, T. Zegers, P. MacKinnon, G. Michael, R. Jaumann, J.-P. Bibring, G. Neukum, and the HRSC Co-Investigator Team. 2006. An integrated study of interior layered deposits in Hebes Chasma, Valles Marineris, Mars, using MGS, MO, and MEX Data. *38th Lunar Planetary Science Convention*, Abstract #2022.

Head, J.W., R. Greeley, M.P. Golombek, W.K. Hartmann, E. Hauber, R. Jaumann, P. Masson, G. Neukum, L.E. Nyquist and M.H. Carr. 2001. Geological Process and Evolution. *Space Science Reviews, 96*: 263-292.

Hynek, B.M., R. Phillips, and R. Arvidson. 2003. Explosive volcanism in the Tharsis region: Global evidence in the Martian record. *Journal of Geophysical Research, 108(E9), 5111, doi*:10.1029/2003JE002062.

Jaumann, R., G. Neukum, T. Behnke, T.C. Duxbury, K. Eichentopf, J. Flohrer, S.V. Gasselt, B. Giese, K. Gwinner, E. Hauber, H. Hoffmann, A. Hoffmeister, U. Köhler, K-D Matz, T.B. McCord, V. Mertens, J. Oberst, R. Pischel, D. Reiss, E. Ress, T. Roatsch, P. Saiger, F. Scholten, G. Schwarz, K. Stephan, M. Wählisch, and the HRSC Co-Investigator Team. 2007. The high-resolution stereo camera (HRSC) experiment on Mars Express: Instrument aspects and experiment conduct from interplanetary cruise through the nominal mission. *Planetary Space Science, 55*: 928-952.

Komatsu, G., G.G. Ori, P. Ciarcelluti, and Y.D. Litasov. 2004. Interior layered deposits of Valles Marineris, Mars: analogous subice volcanism related to Baikal Rifting, Southern Siberia. *Planetary Space Science, 52*: 167-187.

Komatsu, G. and Y. Litasov. 2002. Subice volcanism on the Azas Plateau: a comparison with possible Martian tuyas. *33rd Lunar and Planetary Science Convention*, Abstract #1262.

Komatsu, G., P.E. Geissler, R.G. Strom, R.B. Singer. 1993. Stratigraphy and erosional landforms of layered deposits in Valles Marineris, Mars. *Journal of Geophysical Research, 98*: 11,105–11,121.

Lucchitta, B., N. Isbell, and A. Howington-Kraus. 1994. Topography of Valles Marineris: Implications for erosional and structural history. *Journal of Geophysical Research, 99*: 3783-3798.

Lucchitta, B.K. 1990. Young Volcanic Deposits in Valles Marineris, Mars? *Icarus, 86*: 476-509.

Lucchitta, B.K. and M. Bertolini. 1990. Interior structures of Valles Marineris, Mars. *20th Lunar and Planetary Science Convention*, Abstract #590-591.

Lucchitta, B.K. 1987. Recent mafic volcanism on Mars. *Science, 235*: 565-567.

Malin, M.C., and K.S. Edgett. 2000. Sedimentary rocks of early Mars. *Science, 290*: 927-1938.

Mangold, N., A. Gendrin, C. Quantin, J. Bibring, B. Gondet, Y. Langevin, F. Poulet, R. Arvidson, J. Griffes, E. Hauber, P. Masson, G. Neukum, Omega Team, HRSC Co-Investigator Team. 2007a. An overview of the sulfates detected in the equatorial regions by the OMEGA/MEX spectrometer. *7th International Conference on Mars*, Abstract #3141.

Mangold, N., A. Gendrin, C. Quantin, B. Gondet, J. Bibring, V. Ansan, P. Masson, G. Neukum, OMEGA Team, HRSC Co-Investigator Team. 2007b. Sulfate-rich deposits in West Candor Chasma. *38th Lunar and Planetary Science Convention*, Abstract #1643.

Mangold, N., P. Allemand, P.G. Thomas, G. Vidal. 2000. Chronology of compressional deformation on Mars: evidence for a single and global origin. *Planetary and Space Science, 48*: 1201-1211.

Milliken, R.E., G. Swayze, R. Arvidson, J. Bishop, R. Clark, B. Ehlmann, R. Green, J. Grotzinger, R. Morris, S. Murchie, J. Mustard, and C. Weitz. 2008. Opaline silica in young deposits on Mars. *Geology, 36*: no. 11; p. 847–850; doi: 10.1130/G24967A.1

NASA. 2009. Valles Marineris Flyover. [Online]. *Goddard Space Flight Center.* http://svs.gsfc.nasa.gov/vis/a000000/a001100/a001101/marineris0900_web.jpg. May 25, 2009.

Nedell, S., S. Squyres, and D. Andersen. 1987. Origin and evolution of the layered deposits in the Valles Marineris, Mars. *Icarus, 70*, 409-441.

Peterson, C. 1981. A secondary origin for the Central Plateau of Hebes Chasma. Proc. *12th Lunar and Planetary Science Convention*, Part B, Pergamon Press: New York, 1459-1471.

Peulvast, Jean-Pierre, Daniel Mege, Jan Chiciak, Francois Costard and Philippe Masson. 1994. Morphology, evolution and tectonics of Valles Marineris wall slopes (Mars). *Geomorphology, 37*: 329-352.

Rossi, A.P., G. Neukum, M. Pondrelli, S. Van Gasselt, T. Zegers, E. Hauber, A. Chicarro, and B. Foing. 2008. Large-scale spring deposits on Mars? *Journal of Geophysical Research, 113(EO), 8016,* doi:10.1029/2007JE003062.

Shultz, R. and J. Lin. 2001. Three-dimensional normal faulting models of the Valles Marineris, Mars, and geodynamic implications. *Journal of Geophysical Research, 106*: 16 549-16 566.

Schultz, R.A. 1998. Multiple-process origin of Valles Marineris basins and troughs, Mars. *Planetary Space Science, 46*: 827-834.

Shultz, R:A. 1997. Duel-process genesis for Valles Marineris basins and troughs on Mars. *28th Lunar and Planetary Science Convention,* Abstract #1864.

Solomon, S., O. Aharonson, J. Aurnou, B. Banerdt, M. Carr, A. Dombard, H. Frey, M. Golombek, S. Hauck, J. Head, B. Jakosky, C. Johnson, P. McGovern, G. Neumann, R. Phillips, D. Smith and M. Zuber. 2005. New Perspectives on Ancient Mars. *Science, 307*: 1214-1220.

Vaniman, D. and S. Chipera. 2006. Transformations of Mg- and Ca-sulfate hydrates in Mars regolith. *American Mineralogist; 91*; no. 10; p. 1628-1642

CHAPTER 3 – NORTHERN ILDs

Structural Analysis of Interior Layered Deposits in Northern Coprates Chasma, Mars

F. Fueten[a], H. Racher[a], R. Stesky[b], P. MacKinnon[a], E. Hauber[c], P. C. McGuire[c,e,f], T. Zegers[d], K. Gwinner[c].

[a]Department of Earth Sciences, Brock University, St. Catharines, Ontario, Canada L2S 3A1 < ffueten@brocku.ca>; [b]Pangaea Scientific, Brockville, Ontario, Canada; [c]Institute of Planetary Research, German Aerospace Center (DLR), Berlin, Germany; [d]Faculty of Geosciences, Utrecht University, Utrecht, The Netherlands; [e]Institute for Geosciences, Department of Planetary Science and Remote Sensing, Freie Universitaet, Berlin, Germany; [f]Formerly at: McDonnell Center for the Space Sciences, Washington University, St. Louis, Missouri, USA.

Note: This manuscript is part of a special HRSC volume, in the journal *Earth and Planetary Science Letters*.

Fueten, F., *et al.* Structural Analysis of Interior Layered Deposits in Northern Coprates Chasma, Mars. Earth and Planetary Science Letters. (2009), doi:10.1016/j.epsl.2009 .11.004.

Due to the time constraints of submission, F. Fueten was the lead author with contributions from all authors in the order of authorship. The data is largely based on observations gathered by H. Racher. CRISM data and analysis was provided by P. C. McGuire.

ABSTRACT

Interior layered deposits within an embayment on the northern wall of Coprates Chasma in the Valles Marineris, Mars, are studied using HRSC, CTX, HiRISE and CRISM data. The layered material outcrops in three separate locations. The largest layered deposit within the embayment, a free standing central mound, has an approximate stratigraphic thickness of 2 km. Dip directions change along the central axis of this mound, which is also a zone of deformation. The surface texture of layers within this mound displays polygonal structures at the HiRISE scale. By contrast, the western layered deposit abuts directly against the chasma wall and appears to have a relatively uneroded depositional surface approximately 600 m below the current top elevation of the central mound. A basement ridge, exposed by a landslide scar near the eastern portion of the area, is covered with layered material and shows downward displacement. It is suggested that the entire embayment originated as a small ancestral basin. The displaced basement ridge is evidence of the early basin collapse. The central mound was most likely deposited on a wall rock spur. Deposition did not fill the basin evenly. The detection of hydrated sulfates attests to alteration or deposition by liquid water. Following an erosion event, which coincided with or post-dated the Valles Marineris formation, thin mesa-forming materials covered most of the area.

INTRODUCTION

Interior layered deposits (ILDs) occur throughout the chasmata of the Valles Marineris and account for approximately 17% of the total area and 60% of all chasma deposits (Lucchitta *et al.*, 1994). The origin and mechanism of ILD formation is uncertain. Several hypotheses are proposed, including lacustrine (Nedell *et al.*, 1987), aeolian (Peterson, 1981), pyroclastic volcanism in subaerial (Hynek *et al.*, 2003; Chapman, 2002; Lucchitta, 1987, 1990) or in subglacial (Nedell *et al.*, 1987; Chapman and Tanaka, 2001; Komatsu *et al.*, 2004) environments. More recently it has been suggested that ILDs formed as spring deposits (Rossi *et al.*, 2008). All of these processes imply that the troughs within which the ILDs formed are older than the ILDs. Alternatively, Malin and Edgett (2000) and Catling *et al.* (2006) suggest ILDs are ancient deposits buried beneath the material which form the walls of troughs. The diversity of ILD characteristics implies that several mechanisms were involved in their formation.

The chasmata of the Valles Marineris were likely formed during a two stage process (Lucchitta *et al.*, 1994; Schultz, 1998). Ancestral basins with irregular outlines were proposed to form prior to the opening of the Valles Marineris during rift-like faulting (Lucchitta and Bertolini, 1990; Lucchitta *et al.*, 1994). Lucchitta *et al.* (1994) suggest that Hebes, south Ophir, south Candor and potentially south Melas Chasma were sites of ancestral basins, while much of Coprates, north Melas and Ius may have formed during the later faulting episodes. Faulting resulting from the opening of the Valles Marineris (Schultz, 1998) connected surrounding basins and formed the current canyon configuration.

Mineralogical data from the OMEGA instrument on the Mars Express mission suggest water as a mechanism in the formation or alteration of local ILDs because of the presence of sulfates (Gendrin *et al.*, 2005; Mangold *et al.*, 2007a, b). More recently (Milliken *et al.*, 2008) CRISM data revealed the presence of opaline silica to be associated with some sulfate locations on top of the plateaus surrounding the Valles Marineris troughs. Chojnacki and Hynek (2008) provide a comprehensive review of water-altered minerals within Valles Marineris and suggest that no single formation mechanism can account for the available data. Generally, though not always, monohydrated kieserite occurs on steeper slopes while polyhydrated sulfates often form benches, knobs or hummocky terrain (Chojnacki and Hynek, 2008). The most likely reason for this variation is the relative difference in erosional resistance between mono- and polyhydrated sulfates (Chojnacki and Hynek, 2008).

A recent model for ILD formation, based on stratigraphic and structural observations (Fueten *et al.*, 2008) within western Candor Chasma suggests deposition occurred synchronously with subsidence of early basins and that individual subsiding basin blocks may be identified. According to this model the deposition takes place without the formation of obvious unconformities or disconformities during the subsidence phase, but is followed by a major period of erosion, most likely associated with the linkage of basins and the establishment of drainage channels during the opening of Valles Marineris. Following that period of erosion, there is evidence for only minor subsequent deposition.

In this study, we follow the general methodology of Fueten *et al.* (2008) to study small layered deposits located within an embayment of Coprates Chasma to test the

proposed model. What makes this area particularly interesting is that Coprates Chasma is not one of the prime candidates for an ancestral basin (Lucchitta *et al.*, 1994). It is suggested that while there are significant differences, the overall observations do indeed support the model.

Geological Setting

This study area is located within an embayment on the northern wall of Coprates Chasma (Fig. 3-1). An anaglyph of the area is provided in Figure 3-2. The southern boundary of the embayment is formed by a linear embankment trending approximately 110°. Along this boundary, the base of the embayment is 500 m, 1 km above the floor of Coprates Chasma. The largest volume of layered material within the embayment occurs as a central deposit that is approximately 12 km long and 8 km wide (Fig. 3-1CD). Also present are layered deposits to the west of the main mound (Fig. 3-1WD) and some layered material to the south east of the main mound (Fig. 3-1ED). In contrast to the isolated central mound, the western deposit appears to be directly in contact with the wall. This deposit is approximately 8 km wide and 7 km long. The layered material to the south east (Fig. 3-1ED) within the embayment is located near the site of a major landslide structure and occurs as several small mounds.

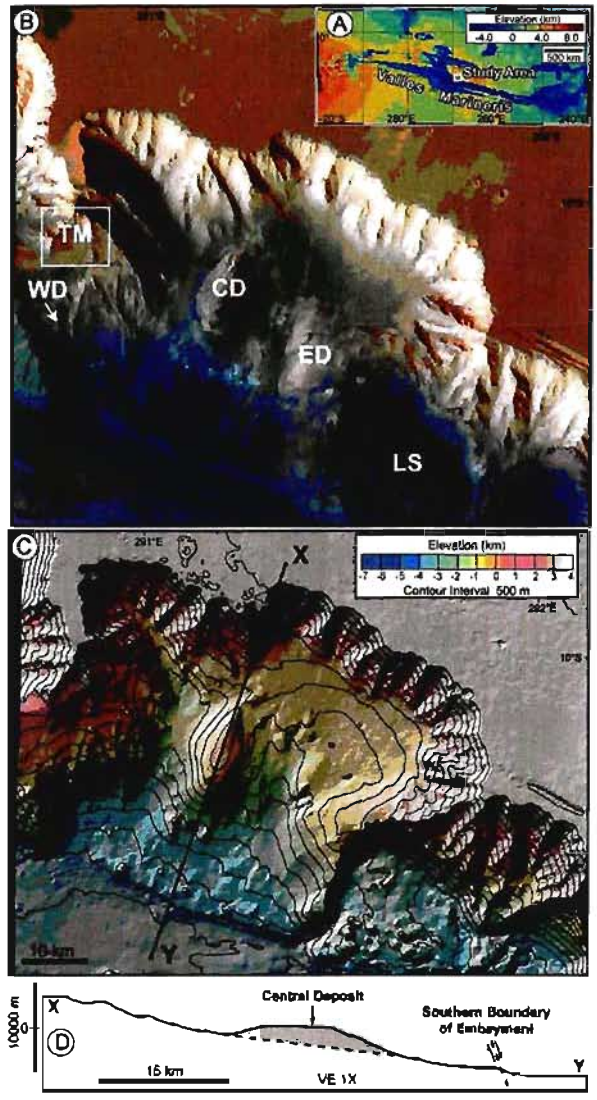

Figure 3-1. Inset A: Location of embayment. Inset B: HRSC colour composite (top) and Inset C: HRSC DEM. Locations WD, CD, ED are locations of Eastern Deposit, Central Deposit and Western Deposit respectively. LS indicates the location of the large landslide. The area TM is the location of Figure 3-3, showing the thin mesa. Inset D: Cross section with no vertical exaggeration along line X-Y as marked within Figure 3-1C. Justification for shading of Central Deposit is provided within the text below. Also labelled on the cross section is the southern boundary of the embayment which is tentatively indicated as a normal fault.

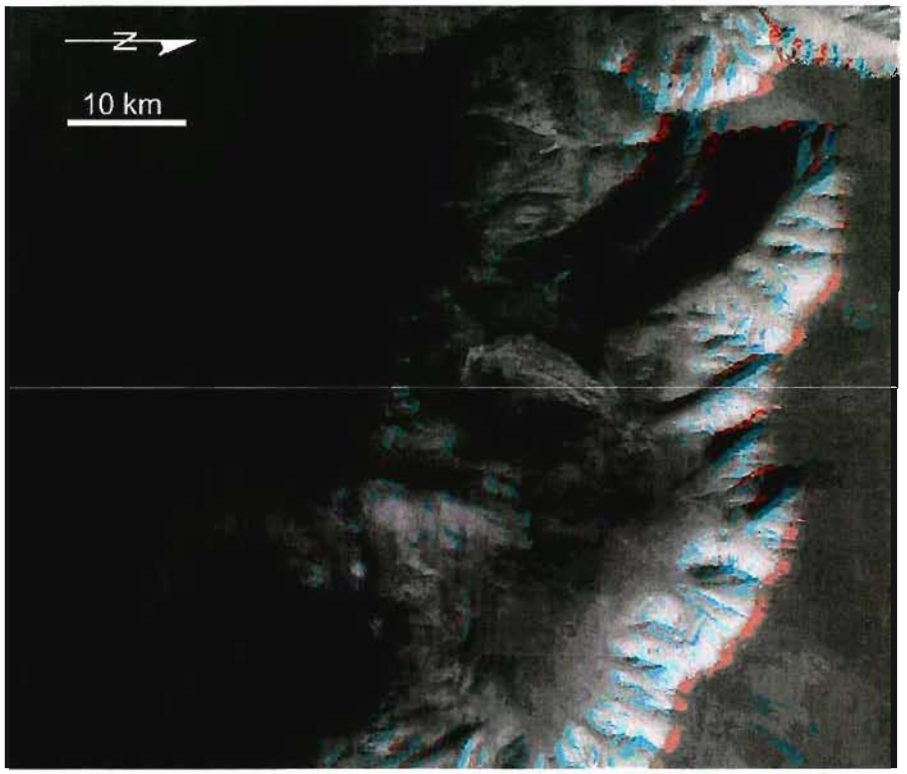

Figure 3-2. Anaglyph of the study area, prepared from HRSC stereo pairs.

Layered deposits within Valles Marineris show a range of layering thicknesses, albedos and erosional characteristics with varying degrees of competency and compositions (Fueten *et al.*, 2008; Rossi *et al.*, 2008; Catling *et al.*, 2006; Hauber *et al.*, 2006; Komatsu *et al.*, 2004; Malin and Edgett, 2000; Komatsu *et al.*, 1993). Malin and Edgett (2000) divide the deposits into three categories; light- to intermediate-toned "layered" units, light- to intermediate-toned "massive" units, and "thin mesa" units, which consist of dark- to intermediate-toned capping units. Adopting this terminology, the three locations discussed above are composed primarily of layered units. As pointed out by Malin and Edgett (2000), thin mesa material here appears to unconformably cover some layered material (Fig. 3-3). Thin mesa materials (Fig. 3-3) also cover significant portions of the chasma walls, where they appear to have been emplaced on wall rock, and are more cratered than the exposed, eroded layered deposits. Their thickness cannot be

resolved using the resolution of the HRSC DEM (Digital Elevation Model), suggesting that it is on the order of meters, rather than tens of meters. Hence, they are different from the massive mesa units discussed by Fueten *et al.* (2008). Due to the unconformable relationship with the layered units, the thin mesa material is younger than the ILD deposits. This study focuses primarily on the underlying layered units, although thin mesa units are discussed briefly.

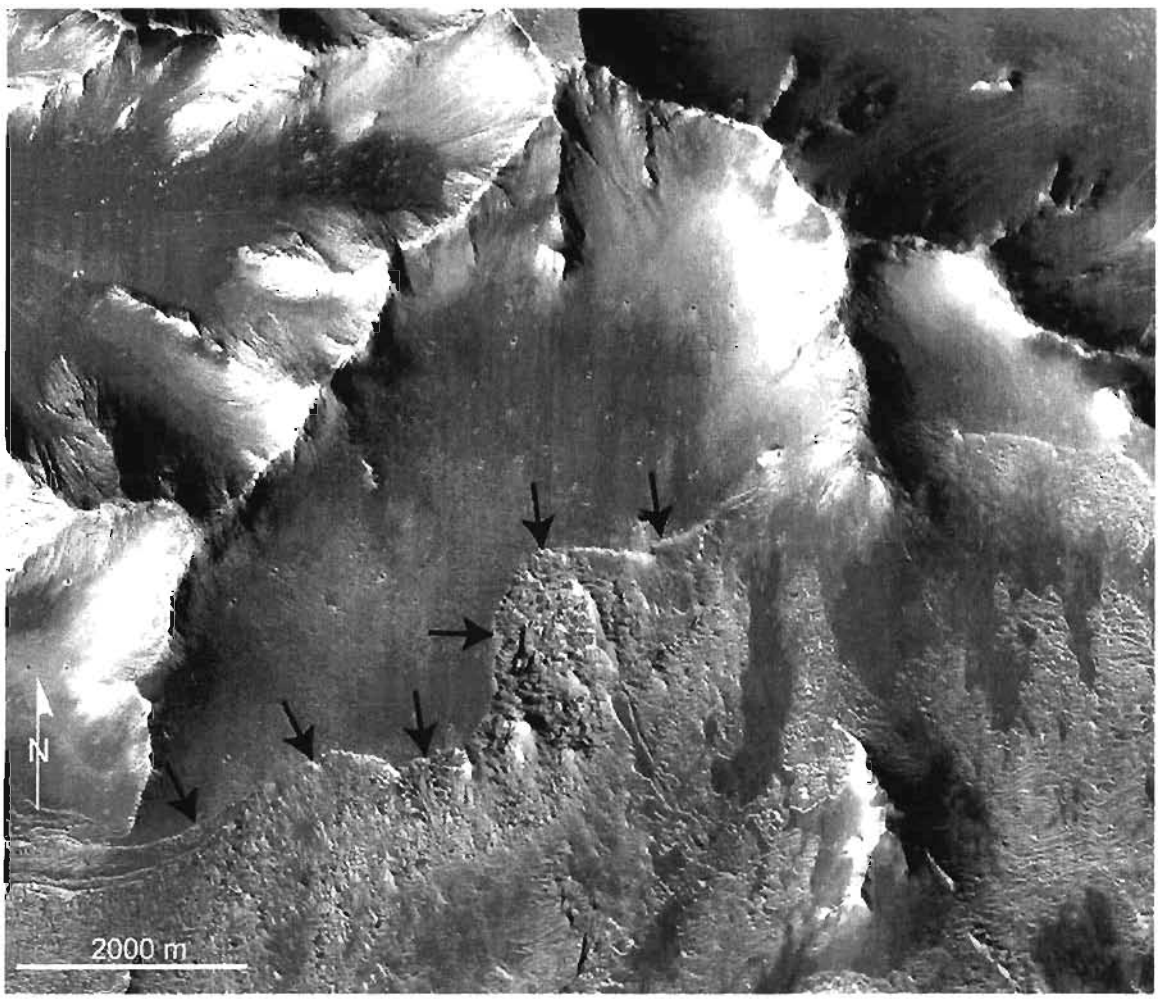

Figure 3-3. CTX mosaic showing thin mesa covering much of the wall rock. Location of this figure as outlined in box labelled TM within Figure 3-1. Black arrows indicate part of the boundary of thin mesa material.

Mineralogical Data Based on CRISM Analysis

We have analyzed CRISM (Murchie *et al.*, 2007) image (HRL00003752) of the central deposit and its surroundings. The CRISM image (HRL00003752) is shown in Figure 3-4, with two spectra shown in Figure 3-5.

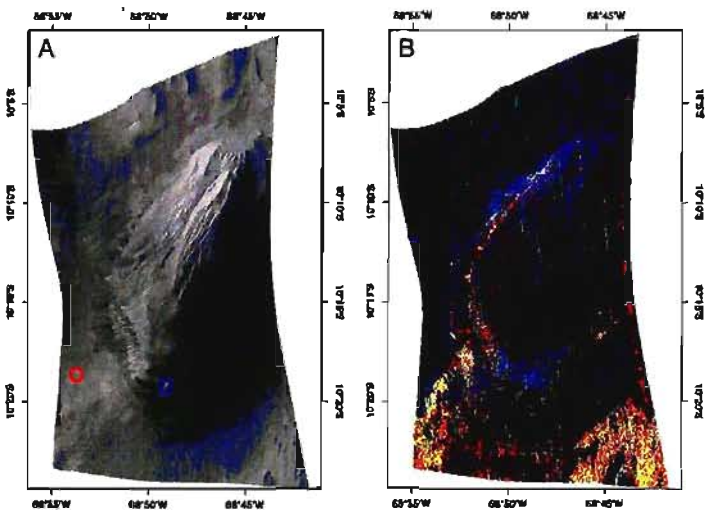

Figure 3-4. For CRISM image HRL00003752 in Coprates Chasma, acquired at L_s = 153°, we show a near-infrared image (Fig. 3-4A) and a sulfate-parameter map (Fig. 3-4B). The near-infrared image has the colour planes (R=2.40 μm, G =2.00 μm, B=1.16 μm), each with a stretch from 0.15-0.40. The locations of the spectra in Figure 5 are indicated by the red circle (mono-hydrated sulfate) and the blue circle (polyhydrated sulfate). The sulfate-parameter map was flattened in order to remove column-dependent variation in the parameters, and it has the colour planes: (R=B2100_flat, G=SINDEX_flat, B=BD1900pcm_flat), with the corresponding thresholds: (0.020, 0.039, 0.036). The conjunction of the red and green colours produces the yellow-coloured regions, which are suggestive of an enhancement of monohydrated sulfates. The conjunction of the blue and green colours produces the cyan-coloured regions, which are suggestive of an enhancement of polyhydrated sulfates.

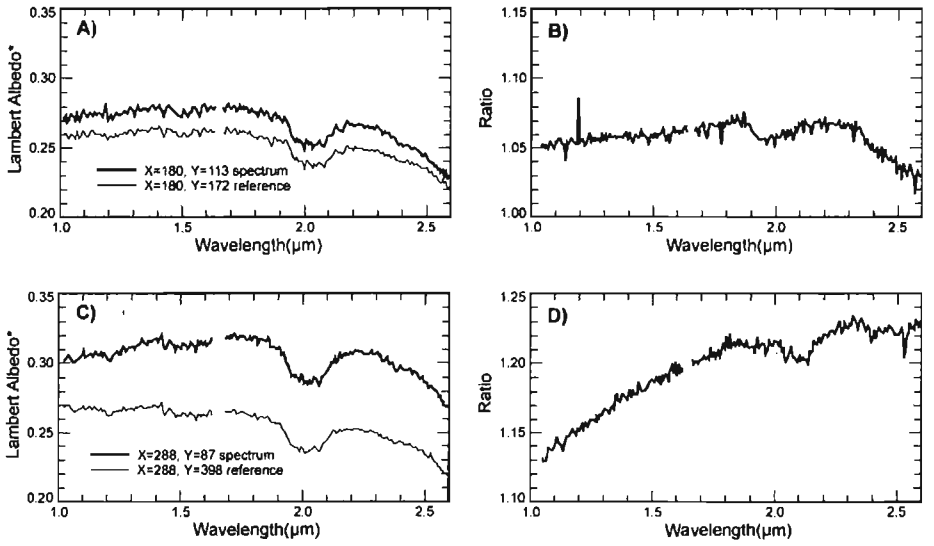

Figure 3-5. For CRISM image HRL00003752 in Coprates Chasma, acquired at L_s = 153°, shown in Figure 3-4, we plot in sub-figures A & C the spectra (bold curves) and the reference spectra (thin curves). The pixel locations in the original image of the spectra and reference spectra are indicated by their X & Y coordinates. All spectra have averaging over a window of 3 × 3 pixel^2. The ratios of the spectra to the reference spectra are shown in subfigure B (corresponding to subfigure A) and in subfigure D (corresponding to subfigure C). For clarity, we have removed noisy spectral data corresponding to a filter boundary near 1.65 μm and a detector boundary near 1.00 μm. The spectra in subfigures A and C have broad absorptions at 1.5 μm and 2.0 μm suggestive of ice-aerosols either in this image or in the volcano-scan transmission spectrum used to correct this image for CO_2 absorption in the atmosphere. The ratio in subfigure B corresponds to the blue circle in the left subfigure of Figure 3-4, and it has an absorption at 1.9 μm and a drop-off at 2.4 μm suggestive of polyhydrated sulfates. The ratio in subfigure D corresponds to the red circle in the left subfigure of Figure 3-4, and it has an absorption at 2.1 μm and a weaker absorption at 2.4 μm suggestive of monohydrated sulfates.

The image was first corrected for CO_2 absorption in the atmosphere by applying an improved version (McGuire *et al.*, 2009) of the 'volcano-scan' atmospheric-correction technique (Langevin *et al.*, 2005) for CRISM and OMEGA data. This improved volcano-scan correction allows the Lambert albedo at 2.01 μm to differ from the Lambert albedo at 1.89 μm, and it also corrects for a slight variation (at the level of < 0.001 μm) in the wavelengths of the CRISM detector, caused by variations in detector temperature (Smith *et al.*, 2008).

Imaging in the near-infrared allows for the detection of minerals in the upper 0.1 mm of a planetary surface. In general (i.e., Murchie *et al.*, 2008), monohydrated sulfates tend to have absorptions at 2.1 μm and 2.4 μm, whereas polyhydrated sulfates tend to have an absorption at 1.9 μm and a drop-off at 2.4 μm. The sulfates can be effectively mapped by spectral summary parameters (Pelkey *et al.*, 2007), in particular the BD1900, BD2100 and SINDEX parameters. The SINDEX parameter detects convexity in the spectra centered at 2.2-2.3 μm due to simultaneous absorption at 1.9-2.1 μm and 2.4 μm. Rather large values were chosen for the thresholds of the spectral summary parameters in Figure 4 in order to cut through some of the apparent effect of ice aerosols on the spectra. With the chosen values for the summary-parameter thresholds, the greatest signal of monohydrated sulfates appear in two large regions on the floor of the chasma (to the south east and to the south west) and a number of discrete locations on the wall of the mound (to the south east and from the south west to the north west). With the chosen values for the summary-parameter thresholds, the greatest signal of polyhydrated sulfates appear on the southern slopes of the mound and on the chasma floor to the north of the northern slopes of the mound.

The use of spectral summary parameters was double checked to map the sulfates in this mound in Coprates Chasma by plotting two spectra (averaged over 3×3 pixel^2) in Figure 5, one spectrum over the polyhydrated-sulfate area on the south slopes of the mound, and one spectrum over a monohydrated-sulfate area on the chasma floor to the south west of the mound. Throughout the image, all the spectra have broad absorptions in them at 1.5 μm and 2.0 μm, suggestive of ice aerosols, which were present either when this image was acquired, or when the volcano-scan transmission spectrum was acquired. By choosing high thresholds for the spectral summary parameters, it can be identified for those places in the image where the sulfates on the surface are visible, despite the obscuring effects of the ice aerosols. Indeed, the maps of sulfate spectral summary parameters do appear to function: ratios of the sulfate-rich spectra to bland spectra in the same detector columns (Fig. 3-5) do contain the corresponding spectral features for sulfates discussed in the previous paragraph.

Several spot checks (not shown here) were conducted of isolated, single pixels on the steep slopes on the west side of the mound which satisfy the thresholds for detection (Fig. 3-4) of both SINDEX and BD2100. These single pixels were located at:

(1) X = 257, Y = 264; with a bland reference pixel at X = 257, Y = 368;

(2) X = 229, Y = 307; with a bland reference pixel at X = 229, Y = 351; and

(3) X = 203, Y = 342; with a bland reference pixel at X = 202, Y = 255.

Spectral ratios of the spectra at these pixels, relative to the bland reference pixels do indeed show bands at 2.1 and 2.4 μm, albeit with somewhat more statistical noise than the spectral ratios shown in Figure 3-5. Therefore, the small, yellow areas on the western

walls of the mound in Figure 3-4 do have monohydrated sulfate signatures similar to the larger yellow areas to the south west of the mound.

Methodology for Attitude Measurements

High Resolution Stereo Camera (HRSC; Jaumann *et al.*, 2007) panchromatic orthoimages, obtained during orbits 2028 and 2039, with a resolution of 12.5 m per pixel and corresponding Digital Elevation Model (DEM) with a grid spacing of 50 m form the primary data set for this study. In addition, a mosaic of three Context Camera images (CTX; Malin *et al.*, 2007) (P02_001865_1697_XI_10S068W, P07_003632_1681_XI_11S068W, P08_004054_1688_XI_11S069W; all with a spatial resolution of 6 m per pixel) was constructed and registered to the HRSC image and hence its corresponding DEM. Layering attitudes were measured on both the HRSC image as well as the CTX composite using the software package Orion following the methodology discussed in detail by Fueten *et al.* (2005). Where the same layer could clearly be identified in both images, measurements on different images were in good agreement (Table 3-1). Due to the higher resolution of the CTX image more layers could be measured within the CTX composite and therefore, with one exception, data presented below is that from CTX images. Layering of the eastern deposit straddles the seam between two CTX images which could not be perfectly matched. Hence, HRSC-based measurements are used for this location.

	HRSC		CTX		HRSC			CTX		
	Strike	Dip	Strike	Dip	# of points	Trace Length (m)	Max. deviation (m)	# of points	Trace Length (m)	Max. deviation (m)
Central Mound	218.7 ± 15.1	4.4 ± 1.4	220.9 ± 17.8	4.5 ± 1.6	8	1398	0.83	16	2197	3.00
	65.8 ± 6.6	14.5 ± 1.8	66.2 ± 7.0	8.4 ± 1.4	10	1704	3.20	8	1311	1.12
	76.6 ± 4.8	10.1 ± 1.2	80.2 ± 7.3	8.8 ± 1.7	9	2423	2.19	11	1443	1.52
	211.6 ± 6.5	13.6 ± 1.8	212.8 ± 7.2	12.2 ± 1.8	9	1591	1.41	13	1368	0.83
	198.2 ± 1.9	17.3 ± 0.7	199.0 ± 3.1	16.5 ± 1.3	8	773	0.23	7	865	0.27
West Deposit	343.6 ± 33.1	9.2 ± 1.7	319.6 ± 11.8	9.8 ± 1.7	7	2062	2.87	11	1765	2.43
	60.2 ± 4.5	18.7 ± 0.9	62.3 ± 7.5	18.4 ± 1.9	6	1460	0.35	11	1204	2.77
East Lobes	127.2 ± 3.2	11.5 ± 0.6	115.9 ± 7.2	12.5 ± 2.1	7	1320	0.32	7	1388	1.59
	179.3 ± 9.4	14.8 ± 1.1	181.7 ± 14.6	14.6 ± 1.6	8	889	1.2	8	1238	3.14
	186.6 ± 8.5	10.1 ± 1.7	174.0 ± 5.9	7.0 ± 1.2	6	957	0.64	7	821	0.40

Table 3-1. Comparison of attitude for layers measured within HRSC and CTX mosaic images from all three deposit locations. Data include: strike and dip measurements with errors, the number of points that were used for each measurement, the trace length over which these points were placed and the maximum deviation for the furthest point from the calculated plane. All planes have correlation coefficients greater than 0.99760.

A HiRISE (High Resolution Imaging Science Experiment; McEwen *et al.*, 2007) image (PSP_001456_1695) was also used for observations but not registered to the DEM because of the large difference in horizontal scale.

OBSERVATIONS

Central Deposit

The long axis of the central deposit is distinctly elevated above the surrounding floor over a distance of 14 km (Fig. 3-6A). South of the steep embankment that forms the obvious edge of the deposit; layers can be seen extending several kilometers further to the south (Fig. 3-7). If these layers are also part of the deposit, then its minimum north-south extent is approximately 17 km. Following similar arguments, its east-west extent is up to 10 km. The top of the deposit is nearly horizontal along the AB section with a slope of less than 1.5° to the south. No contact between the layered deposit and basement (i.e., chasma wall rock) can be identified; hence the base of the deposit could only be estimated. Linking inflection points in the topographic profile along X-Y (Fig. 3-6B); the underlying basement wall rock was estimated to dip uniformly to the south at an angle of 7° (Fig. 3-6C). Using this assumed basement contact, we estimate a stratigraphic thickness of 2 km. The maximum absolute elevation of the central deposit, approximately 200 m, is also the maximum elevation at which layered deposits can be identified within the embayment. This elevation is approximately 3.4 km below the elevation of the plateau (3.6 km). By comparison, other ILD deposits within Valles Marineris occur at elevations of less than 1 km below the local plateau (Quantin *et al.*, 2006; Hauber *et al.*, 2006; Lucchitta *et al.*, 1994).

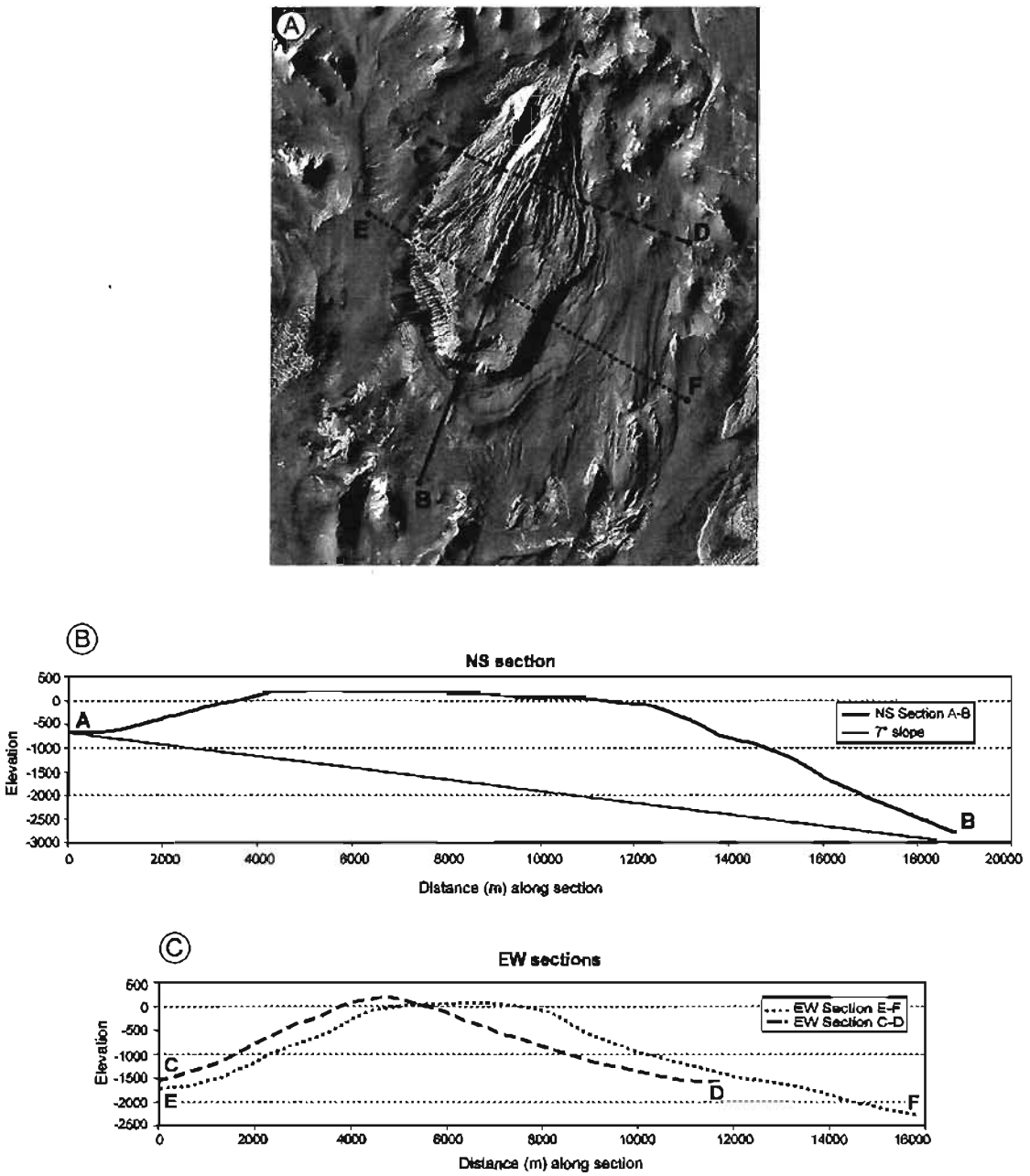

Figure 3-6. Inset A: CTX mosaic of the central deposit, indicating lines of topographic profiles. Inset B: Topographic profiles A-B with no vertical exaggeration. The 7° slope is compatible with slope estimates surrounding the mound. It was chosen to yield a minimum estimate of layered deposit thickness for a constant slope. The same 7° slope was also used for the cross section in Figure 3-1C. Inset C: Topographic profiles C-D and E-F with no vertical exaggeration.

Figure 3-7. Layer attitudes on the central mound. Also indicated are two fault planes discussed below. A, B, C, indicate location of images in Figure 3-8 A, B and C respectively. Black arrows indicate examples of linear scarps discussed below.

The layering attitudes within the central deposits appear to vary systematically with location as well as stratigraphic position. Layers east of the long axis of the deposit dip to the east, while those on the west side dip westerly. Layers lower in the stratigraphy tend to dip more steeply than those at higher elevations and layering on the top of the

mound is nearly horizontal with a dip between 2° and 6°. The layering in the lower west and east stratigraphy dips between 10° and 20°. Layering to the far west dips the steepest with an angle in the range of 20° to 35°. As stated above, layering exposed at the base of the mound appears to be largely covered by thin mesa. This layering cannot be measured with any accuracy. The difficulty of measurement could be due to the mesa covering, or because the layering has been deposited on an uneven substrate making its orientation highly variable over short distances.

Layering as observed in HiRISE image PSP_001456_1695 appears as banded light and dark lithologies (Fig. 3-8A). Some of the dark layers are surficial material that has accumulated on the ledges of more resistant layers, while other layers can be distinguished by different densities of fractures (Fig. 3-8B). Using the horizontal width of layers displayed within the HiRISE image and inclination of the local slope from the HRSC DEM, we can estimate the layer thicknesses. Thickness of dark layers ranges from approximately 2.5 m to 7 m while light layers are generally thicker, ranging from approximately 6.5 m to 11 m. Primarily the light layers are disrupted into polygons, the smallest of which are near the 25 cm/pixel resolution of the HiRISE image. Most polygons range in size from approximately 3 m to 7 m in diameter. The boundaries of the polygons commonly show parallel alignment suggesting tectonic influence (Fig. 3-8AB). Similar, though less deformed, polygons have been described within light toned layering in HiRISE images by Weitz *et al.* (2008) and Pondrelli *et al.* (2008). Pondrelli *et al.* (2008) suggests the light toned beds were disrupted into polygons through tectonic stress or thermal contraction and later deformed. Weitz *et al.* (2008) proposes thermal contraction or desiccation of hydrated minerals as a possible formation mechanism.

Schieber (2007) argues that a structure size of approximately 1 m to 6 m is too large to have resulted from the desiccation cracking of mudstone.

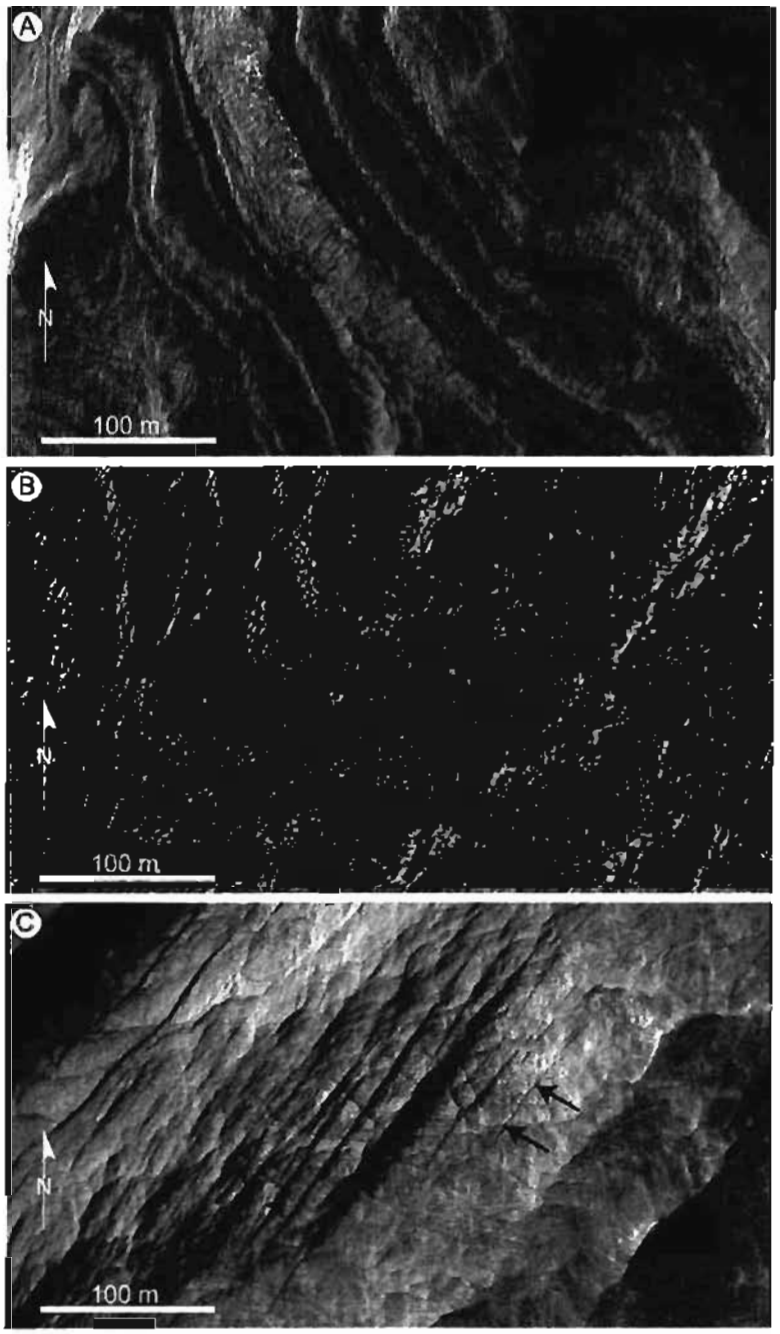

Figure 3-8. HiRISE image PSP_001456_1695. Inset A: Light and dark layering with polygonal structures. Inset B: Disrupted layering with polygonal structures. Inset C: Fracture sets on the east side of the mound. Black arrows point to examples of fractures.

A zone of deformation has been traced as trending approximately 025°, along the long axis of the mound (Fig. 3-7). Layering appears to be more deformed to the west of the zone of deformation. The disturbed layering appears to be smoothly folded (Fig. 3-8B) and no significant or consistent offsets between layering can be detected. The zones of disruption may be similar to bounding bands (Okubo *et al.*, 2009) though the sectioning effect of gently dipping topography and layers likely make the disruption appear to be more severe than it is.

A series of linear scarps are displayed on either side of the central mound (Fig. 3-7). The scarps appear to steeply cut the shallow layering, though the difference in the scale of the scarps and the DTM do not allow for the measurement of the dip of any particular scarp. East of the central axis of the mound these scarps trend between 020° to 040°, while west of the mound the scarp trend is in the 350° to 015° range. They are symmetrical about the zone of disrupted layering that runs down the central axis of the mound. The linearity and consistent attitude on either side of the mound suggest that these scarps are related to the faulting along the central axis.

The north east portion of the mound has two planar surfaces cutting the stratigraphy with similar orientations of 220°/33° for the one spanning the lower stratigraphy level and 223°/33° for the one covering the higher elevations (Fig. 3-7). The strike-parallel extent of the planar portion of these surfaces is approximately 2.5 km for the lower one and 2 km for the upper. Similar features within western Candor Chasma have been interpreted as fault planes (Fueten *et al.*, 2008; Fueten *et al.*, 2007).

Also visible within the HiRISE images are fracture sets (Fig. 3-8C) which appear to be more prominent in the eastern portion of the mound. Here, two perpendicular

fracture sets occur with south west - north east and north west - south east orientations. The south west – north east fracture set is dominant with longer fractures. The fracture sets do not offset layering and appear to be similar to those described by Okubo and McEwen (2007) within a finely layered sequence of ILD material with a kieserite signature. Okubo and McEwen (2007) suggest that sub-surface fluid flow was responsible for the alteration of rocks in the fracture zone and its surroundings.

Western Deposit

The western deposit is not free standing; the northern edge of its main body directly abuts against chasma wall rock. A smaller, free standing mound is located to the south of the main body (Fig. 3-9). As seen in the central mound, layering covered by thin mesa material can be identified south of the elevated layered material. The top surface of the mound is partially covered by the thin mesa unit. This surface is also very planar and parallel to layering visible beneath it, dipping approximately 15° to the south west. The absolute elevation of this surface ranges from approximately -1200 m at its southern extent to approximately -800 m at its northern extent. A distinct change in albedo occurs approximately 200 m below the top surface on the southernmost face of the exposure. The surface defining this change dips 10° to the north east. Layering cannot be clearly identified or measured below this surface. The darker material above this surface appears to be more massive and differs from the generally light toned layered deposits in this embayment. It may be similar to massive units described by Malin and Edgett (2000) or Fueten *et al.* (2008), making it the only such unit within this embayment.

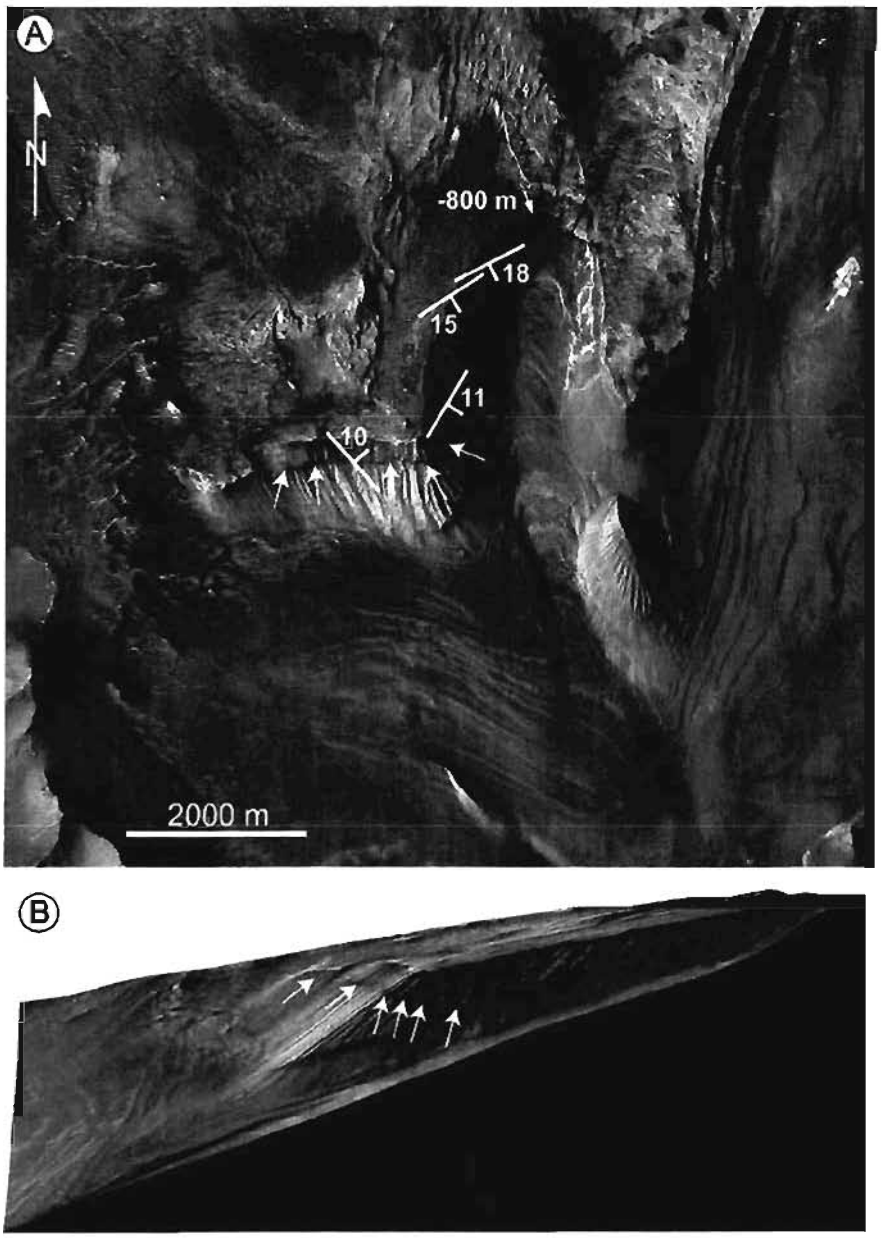

Figure 3-9. Inset A: Map view of Eastern ILD with CTX mosaic. Arrows point to change in albedo, this contact dipping 10° to the north east as indicated. Layering above the contact dips 11° to 18° to the south west as indicated. Inset B: 3D view from the east with no vertical exaggeration. Arrows indicate contact of albedo change. The location of the -800 m elevation discussed within the text is indicated.

Eastern Deposit

Layered deposits within the eastern ILD of the embayment consist of several small mounds (Fig. 3-10). They are surrounded by a larger region of visible layering from which no attitude measurements could be obtained. Thin mesa material appears to cover layered units along much of the edge of the larger region. The regional slope dips approximately 16° to the south west. Only one measurement of the larger, basal layering could be obtained and it is nearly parallel to the regional slope. As stated above, irregularity within the substrate over which the layered material was deposited may account for the lack of measurements. On one of the mounds, two layer measurements indicate dips of 20° and 24° towards the south. Near the edge of the slump structure, fine layered material appears to dip shallowly to the west or south west. A small remnant of thin mesa material dips 9° to the west.

Figure 3-10. Inset A: CTX mosaic displaying layering within the eastern portion of the embayment. Layering of basement ridge indicates a gentle south east plunging fold. Inset B: 3D view with no vertical exaggeration, illustrating the curvature of the central basement ridge.

In the south eastern portion of the area a large landslide has exposed a section of chasma wall rock which displays layering at an elevation of approximately -1 km, 4.5 km below the local plateau elevation (Fig. 3-10). This layering, although well exposed, cannot be measured because it is non-planar. The ridge in the central portion of wall rock in Figure 3-10B is 200 m to 400 m lower in elevation in the center than it is on either end, forming a depression. While no plane can be fitted through the entire trace of this exposure, the south western and north eastern portions of this ridge can be approximated to be planar. The south western portion dips 7° to the north east, while the north eastern portion dips 19° to the south west, forming the geometry of a gentle south easterly plunging fold.

The central wall rock portion is covered by layered material. The lowest levels of this material conform to the wall rock geometry, paralleling the depression, while the upper layers are less curved giving the impression that this layering has filled in the depression. The layered unit is capped by thin mesa material which dips 8° to 9° to the east.

DISCUSSION

Mineralogical Data

In other areas of Valles Marineris, it appears (i.e., Mangold *et al.*, 2008) that the stronger monohydrate sulfates are more common in steeper parts of layered deposits whereas weaker polyhydrated sulfates appear to be less common in steeper portions of layered deposits. Herein, it is not identified the type of monohydrated sulfates. However, for reference, typical examples of monohydrated sulfates include kieserite and szomolnokite. The results of the analysis of this image of the mound in Coprates Chasma appear to be largely consistent with monohydrated sulfates being more common in wall rock than polyhydrated sulfates. The signal for monohydrated sulfates appears to be more common than the signal for polyhydrated sulfates in the steeper slopes on the west side of the mound. Polyhydrated sulfates also appear in the mound on the southern flank, but the slopes there appear to be shallower, in general. Hence, the data in this area appear to follow the general trends observed by Chojnacki and Hynek (2008).

Early Basin

It has been suggested that layered deposits are deposited in early ancestral basins, which are later linked during the formation of Valles Marineris (Lucchitta *et al.*, 1994; Schultz, 1998). The wall embayment in which layered deposits examined here are located is one of the largest along the northern wall of Coprates Chasma and has a complex geometry. While other slump-related embayments open into the chasma (i.e., they get wider towards the chasma), the curvature of this embayment actually narrows in the direction of the chasma (Fig. 3-1AB). The linear nature of the southern boundary of

the embayment and the associated drop in elevation suggests that it is formed by one of the major faults associated with Valles Marineris tectonism (Schultz and Lin, 2001; Mège and Masson, 1996). The size of the embayment is comparable to the size of several small basins within the Tharsis Plateau (e.g., eastern Tithonium). The layered deposits occur at elevations within the approximate range of -1 km to -3 km which is the same range of depths of these isolated basins on the Tharsis Plateau, but well above the local floor of Coprates Chasma (-5.5 km). Hence, it is suggested that this embayment represents the remnants of a small ancestral basin. The exact geometry of this basin is not known since the main Valles Marineris opening removed its southern portion, leaving the northern remnant in its present position.

If the embayment is indeed part of an ancestral basin, an interesting suggestion can be offered for the wall rock deformation described above that has been exposed by the large landslide in the south eastern corner of the area. The wall rock depression is overlain by a sequence of layered material which decreases in curvature up the stratigraphic section and is capped by a planar thin mesa unit. This observation suggests that the depression pre-dates the deposition of layered material. It will be argued later that ILD deposition predates the linking of basins and the opening of the main linear troughs of Valles Marineris. If deposition of layered material is linked to the basin formation, the observed wall rock deformation may thus be the result of early basin collapse. It has been speculated that the size of collapsing floor segments would likely have been several square kilometers in area (Fueten *et al.*, 2008). The displaced wall rock segment is approximately 2 km in width and would thus dimensionally fit well.

Deposition of Layer Deposits

Layering of the central deposit is more inclined at lower stratigraphic levels, while dip measurements near the top of the mound are nearly horizontal, as is the actual erosional surface. None of the basal layering attitudes at any of the three locations could be measured with confidence, suggesting that these layers are not planar. These observations are compatible with layered material that is initially deposited on an inclined, irregular surface, such as the exposed wall rock slopes on the edges of the chasma. In this scenario, basal layers draping over the irregular surfaces would not be planar and planar layering could only be expected after some stratigraphic thickness had been built up. The steeper dips of 20° to 35° are similar to the slopes that can be measured on the sides of wall rock spurs, which may be similar to the basement beneath the layered deposits. The geometry of the eastern deposit suggests that it was deposited directly against wall rock and thus would have to conform to it at its base. While its basal layers could not be measured, wall slope measurements surrounding the deposit range from 10° to 25°.

A gradual decrease in dip at higher stratigraphic levels would be expected in a depositional setting in which externally delivered material is deposited on an inclined surface. This contrasts directly with the expected geometry in which a mound is built up from an internal material source. In such an environment, e.g. a volcano or spring deposit layering dip might be expected to increase higher in the section. However, as pointed out by Rossi *et al.* (2008) the geometry of spring deposits may be very complex.

A zone of deformation transects the central mound, trending approximately 20°. Layer dip directions differ on either side of this zone, as does the average trend of the

larger scarps. However, no significant offsets can be observed across the layering. Hamelin *et al.* (2008) suggested that an active fault, trending approximately 025°, was located near the center of the central mound and that tectonism continued beyond deposition after the mound had lithified. The lack of significant offsets suggests that fault motion was minor. While it may be possible that a fault lies beneath the central axis of the central mound, no evidence for the extension of such a fault north or south beyond the mound was found.

An alternative suggestion is that the central mound material was deposited on top of a wall spur and dip directions on either side of the mound simply mimic those of the underlying wall rock dip. Compaction and quakes during tectonism could then account for some of the disruption along the central axis as material would tend to move down the local underlying wall rock slope. In this scenario, the linear scarps are most likely tensile features, produced by the motion of material, either during tectonism or simply compaction. This argument is also not without problems because in typical spur geometry, strike directions on either side of the spur converge down slope. Gravity driven tensile features would be expected to mimic this geometry. However, the orientations of the linear scarps show the opposite sense of convergence. The elevation north of the mound is approximately 1 km higher than the elevation south of the mound, leaving no doubt as to the wall rock slope. Hence, an underlying wall rock spur would require an unusual geometry to fit the observations. Nevertheless, in the complete absence of any data on the underlying basement geometry, this interpretation for its overall simplicity is favoured.

One important aspect to consider is the original extent of these deposits. The discussions above have focused on exposed layered deposits. However, the north western portion of the embayment is covered by thin mesa material and devoid of the rugged wall rock spurs. This region has an absolute elevation of approximately -300 m, below the maximum height at which layered deposits occur within the embayment and slopes between 7° and 10°. It has already been suggested that thin mesa units have thicknesses on the order of meters and are thus unlikely to be able to cover and smooth out wall rock topography with irregularities (e.g. spurs) on the order of tens to hundreds of meters. Hence, it is possible that this region is also covered by layered deposits which are themselves covered by thin mesa material.

All three deposits show clear signs of erosion. The small mounds of the eastern deposit may well have been linked, but their current appearance does not provide any evidence to suggest their original extent. The top surface of the western deposit however is very planar and parallel to layering underneath it. It may thus represent, or closely resemble, the top of the original depositional surface. Its maximum elevation of approximately -800 m is approximately 600 m below the maximum elevation of the central mound. This suggests it is unlikely that the entire ancestral basin represented by this embayment was filled to the same level. The current geometry of the embayment indicates that the western deposit was within the same basin as the central mound. Many of the larger ILDs studied (Fueten *et al.*, 2008; Hauber *et al.*, 2006) exceed the area of this embayment and appear to have subhorizontal layering that extends for many kilometers. This observation suggests an efficient transport mechanism capable of depositing large volumes evenly over large areas. By contrast, the observations here

imply that these transport mechanisms were incapable of, or not available for, the even distribution of material throughout the basin.

Post-ILD Deposition and Erosion

As discussed above, the ILDs have been affected by erosion. At the very least, this erosion removed approximately 500 m of thickness from the south eastern edge of the central mound to create the cliff on the south east side. Only a small debris apron surrounds the central mound and what appear to be basal layers of the deposits are visible over a wide extent of the embayment far beyond the topographic expression of the mound. In addition, a significant volume would have been removed during the faulting or slumping that created the 2 km to 2.5 km long scarps on the north western edge of the central mound. This observation suggests that a significant erosion event affected these layered deposits and a large volume of eroded material has been removed from the embayment. This extent of erosion is difficult to accomplish while the ancestral basin is closed and hence, most likely occurred while Coprates Chasma was forming, or had already formed.

Thin mesa material covers much of the embayment, masking layered material in many locations but also showing signs of erosion. The similarity of the appearance of the thin mesa material throughout the embayment suggests that it was initially deposited as a thin, relatively uniform sheet over the entire embayment. It is unlikely that the embayment was filled with standing water after the downward movement of the linear trough which connected it to Coprates Chasma. This would also require the chasma and all connected basins to be filled to the same level. Hence, the most likely mode of

forming a uniform sheet of thin mesa is by airborne ash fall. It is quite likely that the thin mesa-producing event occurred repeatedly throughout the geological history. The thin mesa material is now preserved primarily on the wall slopes and on relatively flat regions. The absence of thin mesa from areas of local high elevation, such as the mounds, can be explained by more active wind erosion in those localities. Since thin mesa material covers much of the wall slopes; most of the geometry of the walls of the embayment has probably not been modified since the latest thin-mesa deposition event.

Timing of Events

The evidence suggests that ILD materials along the northern wall of Coprates Chasma were deposited in a small ancestral basin. Lower basal layers are thought to drape over an irregular underlying wall rock topography making them younger than the local wall rock of the embayment. The observations of the layered material do not lead to any direct conclusions about the mode of deposition, although the significant differences in top elevations between western and central deposits suggest that the transport mechanisms were incapable of distributing the layered material evenly throughout the embayment. The full geometry of the basin and its southern extent cannot be inferred. Lucchitta (1994) and Fueten *et al.* (2008) argue that ILD deposition took place during early basin formation and prior to Valles Marineris formation. Fueten *et al.* (2008) suggests that the opening of Valles Marineris coincided with the cessation of deposition and a major erosion event. The observations presented here are compatible with the timing of that model. As has been argued above, the depositional extent of the layered deposits exceeded their present extent which indicates a significant erosion event. Since

this eroded material has not been re-deposited within the embayment, it must have been removed into the main part of Coprates Chasma or beyond. Hence, Coprates Chasma must have existed or was in the process of forming during the erosional event. Thin mesa material covers eroded layering and thus represents the latest event. Since this is a thin covering, the volume of deposited material following the opening of the main linear troughs of Valles Marineris is minor. This conclusion agrees with the suggestion of Fueten *et al.* (2008) that erosion, most likely linked to VM opening, was followed by only minor deposition.

CONCLUSION

Layered deposits within an embayment on the northern slope of Coprates Chasma most likely formed within a small ancestral basin. The deposits were emplaced upon an irregular wall rock basement and hence post-date the basement. While it is not possible to identify the mode of deposition, transport mechanisms were incapable of distributing the layered material evenly throughout the embayment. A small segment of wall rock that has been displaced downward with respect to its surroundings and covered by layered material provides the first direct visual evidence of basement collapse. Water must have been present to explain the existence of hydrated sulfates. It is impossible to identify the source of the water (precipitation versus groundwater or hydrothermal fluids). Mineralogical evidence is consistent with trends observed elsewhere with monohydrated sulfates being more common on steeper slopes. Following the deposition a significant period of erosion took place. The eroded material was removed from the embayment, most likely during or after Coprates Chasma had formed. Thin mesa most likely formed as airborne ash fall as a regionally extensive sheet and has been partially eroded since then. Since thin mesa material still covers much of the wall slope, the wall rock geometry has not been modified significantly following the last thin mesa deposition. While there are substantial differences between this study area and west Candor Chasma, the observations here are compatible with the model for ILD formation proposed by Fueten *et al.* (2008).

ACKNOWLEDGEMENTS

We thank the HRSC Experiment Teams at DLR Berlin and Freie Universitaet Berlin, and the Mars Express Project Teams at ESTEC and ESOC for their successful planning and acquisition of data, as well as for making the processed data available to the HRSC Team. We also want to thank the CTX, HiRISE and CRISM Teams for making their data available. This project was partially funded by an NSERC discovery grant to F. Fueten. Pangaea Scientific thanks P. Budkewitsch and Canada Centre for Remote Sensing for support of ORION under contract NRCan-01-0102. The work by P.C. McGuire has been funded by a Robert M. Walker senior research fellowship from the McDonnell Center for the Space Sciences, by a Humboldt Research Fellowship, and by support from NASA funds through the Applied Physics Laboratory, under subcontract from the Jet Propulsion Laboratory through JPL Contract #1277793. This study was also partly supported by the Helmholtz Association through the research alliance "Planetary Evolution and Life". We thank M. Lozon for preparing the illustrations. We appreciate a thorough review by Chris Okubo.

REFERENCES

Catling, D.C., S.E. Wood, C. Leovy, D.R. Montgomery, H.M. Greenberg, C.R. Glein, J.M. Moore. 2006. Light-toned layered deposits in Juventae Chasma, Mars. *Icarus, 181*: 26-51.

Chapman, M.G., and K.L. Tanaka. 2001. Interior trough deposits on Mars: Subice volcanoes? *Journal of Geophysical Research, 106(E5)*: 10,087-10,100.

Chapman, M.G. 2002. Layered, massive, and thin sediments on Mars: Possible Late Noachian to Late Amazonian tephra? In: Smellie, J.L. and M.G. Chapman, (eds). Volcano-Ice Interactions on Earth and Mars. *Geological Society, London, Special Publications, 20*: 273-203.

Chojnacki M. and B.M. Hynek. 2008 submitted. The geological context of water-altered minerals in Valles Marineris, Mars. *Journal of Geophysical Research.*

Fueten, F., R. Stesky, P. MacKinnon, E. Hauber, T. Zegers, K. Gwinner, F. Scholten, and G. Neukum. 2008. Stratigraphy and structure of interior layered deposits in west Candor Chasma, Mars, from High Resolution Stereo Camera (HRSC) stereo imagery and derived elevations. *Journal of Geophysical Research, 113, E10008, doi*:10.1029/2007JE003053.

Fueten, F., R. Stesky, P. MacKinnon, E. Hauber, T. Zegers, K. Gwinner, F. Scholten, and G. Neukum and the HRSC Co-Investigator Team. 2007. Faulting of ILD deposits on Ceti Mensa, Western Candor Chasma, Mars. *38th Lunar and Planetary Science Convention*, Abstract #1388.

Fueten, F., R.M. Stesky, and P. MacKinnon. 2005. Structural attitudes of large scale layering in Valles Marineris, Mars, calculated from Mars Orbiter Laser Altimeter data and Mars Orbiter Camera imagery. *Icarus, 175*: Issue 1, 68-77.

Gendrin, A., N. Mangold, J. Bibring, Y. Langevin, B. Gondet, F. Poulet, G. Bonello, C. Quantin, J. Mustard, R. Arvidson, and S. LeMouélic. 2005. Sulfates in Martian layered terrains: The OMEGA/Mars Express view. *Science, 307*: 1587-1591.

Hamelin, H., H. Racher, F. Fueten, R. Stesky, P. MacKinnon, E. Hauber, K. Gwinner, F. Scholten, T. Zegers. 2008. Structural analysis of an interior layered deposit in Northern Coprates Chasma, Mars. *39th Lunar and Planetary Science Convention*, Abstract #1424.

Hauber, E., K. Gwinner, A. Gendrin, F. Fueten, R. Stesky, S. Pelkey, H. Wulf, D. Reiss, T. Zegers, P. MacKinnon, G. Michael, R. Jaumann, J.-P. Bibring, G. Neukum, and the HRSC Co-Investigator Team. 2006. An integrated study of interior layered deposits in Hebes Chasma, Valles Marineris, Mars, using MGS, MO, and MEX Data. *37th Lunar and Planetary Science Convention*, Abstract #2022.

Hynek, B.M., R.J. Phillips, and R.E. Arvidson. 2003. Explosive volcanism in the Tharsis region: Global evidence in the Martian record. *Journal of Geophysical Research, 108(E9)*: 5111, doi:10.1029/2003JE002062.

Jaumann, R., G. Neukum, T. Behnke, T.C. Duxbury, K. Eichentopf, J. Flohrer, S.V. Gasselt, B. Giese, K. Gwinner, E. Hauber, H. Hoffmann, A. Hoffmeister, U. Köhler, K-D Matz, T.B. McCord, V. Mertens, J. Oberst, R. Pischel, D. Reiss, E. Ress, T. Roatsch, P. Saiger, F. Scholten, G. Schwarz, K. Stephan, M. Wählisch, and the HRSC Co-Investigator Team. 2007. The high-resolution stereo camera (HRSC) experiment on Mars Express: Instrument aspects and experiment conduct from interplanetary cruise through the nominal mission. *Planetary Space Science, 55*: 928-952.

Komatsu, G., G.G. Ori, P. Ciarcelluti, and Y.D. Litasov. 2004. Interior layered deposits of Valles Marineris, Mars: analogous subice volcanism related to Baikal Rifting, Southern Siberia. *Planetary Space Science, 52*: 167-187.

Komatsu, G., P.E. Geissler, R.G. Strom, and R.B Singer. 1993. Stratigraphy and erosional landforms of layered deposits in Valles Marineris, Mars. *Journal of Geophysical Research, 98*: 11,105–11,121.

Langevin, Y., F. Poulet, J.-P. Bibring and B. Gondet. 2005. Sulfates in the north polar region of Mars detected by OMEGA/Mars Express. *Science, 307*: (5715), pp.

1584-1586.

Lucchitta, B.K., N.K. Isbell, and A. Howington-Kraus. 1994. Topography of Valles Marineris: Implications for erosional and structural history. Journal *of Geophysical Research, 99*: 3783-3798.

Lucchitta, B.K. 1990. Young volcanic deposits in the Valles Marineris, Mars? *Icarus, 86*: 476-509.

Lucchitta, B.K and M.L. Bertolini. 1990. Interior structures of Valles Marineris, Mars. *20th Lunar and Planetary Science Convention*, Abstract #590-591.

Lucchitta, B.K. 1987. Recent mafic volcanism on Mars. *Science, 235*: 565-567.

Malin, M.C., J.F. III Bell, B.A. Cantor, M.A. Caplinger, W.M. Calvin, R.T. Clancy, K.S. Edgett, L. Edwards, R.M. Haberle, P.B. James, S.W. Lee, M.A. Ravine, P.C. Thomas, and M.J. Wolff. 2007. Context Camera Investigation on board the Mars Reconnaissance Orbiter. *Journal of Geophysical Research, 112, CiteID E05S04, doi*: 10.1029/2006JE002808.

Malin, M.C., and K.S. Edgett. 2000. Sedimentary rocks of early Mars. *Science, 290*: 927-1938.

Mangold, N. A. Gendrin, B. Gondet, S. LeMouelic, C. Quantin, V. Ansan, J.-P. Bibring, Y. Langevin, P. Masson and G. Neukum. 2008. Spectral and geological study of the sulfate-rich region of West Candor Chasma, Mars. *Icarus, 194(2)*: pp. 519-543.

Mangold, N., A. Gendrin, C. Quantin, J. Bibring, B. Gondet, Y. Langevin, F. Poulet, R. Arvidson, J. Griffes, E. Hauber, P. Masson, G. Neukum, Omega Team, HRSC Co-Investigator Team. 2007a. An overview of the sulfates detected in the equatorial regions by the OMEGA/MEX spectrometer. *7th International Conference on Mars*, Abstract #3141.

Mangold, N., A. Gendrin, C. Quantin, B. Gondet, J.-P. Bibring, V. Ansan, Ph. Masson, G. Neukum, OMEGA Team, HRSC Co-Investigator Team. 2007b. Sulfate-rich deposits in West Candor Chasma. *38th Lunar and Planetary Science Convention*, Abstract #1643.

McEwen, A.S., E.M. Eliason, J.W. Bergstrom, N.T. Bridges, C.J. Hansen, W.A. Delamere, J.A. Grant, V.C. Gulick, K.E. Herkenhoff, L. Keszthelyi, R.L. Kirk, M.T. Mellon, S.W. Squyres, N. Thomas and C.M. Weitz. 2007. Mars Reconnaissance Orbiter's High Resolution Imaging Science Experiment (HiRISE). *Journal Geophysical Research, 112, CiteID E05S02, doi*: 10.1029/2005JE002605.

McGuire, P.C., J.L. Bishop, A.J. Brown, A.A. Fraeman, G.A. Marzo, M.F. Morgan, S.L. Murchie, J.F. Mustard, M. Parente, S.M. Pelkey, T.L. Roush, F.P. Seelos, M.D. Smith, L. Wendt, and M.J. Wolff. 2009 submitted. A new volcano-scan algorithm for atmospheric correction of CRISM and OMEGA spectral data.

Mège, D. and P. Masson. 1996. Amounts of crustal stretching in Valles Marineris, Mars. *Planetary Space Science, 44*: 749-782.

Milliken, R.E., G.A. Swayze, R.E. Arvidson, J.L. Bishop. R.N. Clark, B.L. Ehlmann, R.O. Green, J.P. Grotzinger, R.V. Morris, S.L. Murchie, J.F. Mustard, and C. Weitz. 2008. Opaline silica in young deposits on Mars. *Geology, v. 36; no. 11; p. 847–850; doi*: 10.1130/G24967A.1

Murchie, S., R. Arvidson, P. Bedini, K. Beisser, J.-P. Bibring, J. Bishop, J. Boldt, P. Cavender, T. Choo, R.T. Clancy, E.H. Darlington, D. Des Marais, R. Espiritu, D. Fort, R. Green, E. Guinness, J. Hayes, C. Hash, K. Heffernan, J. Hemmler, G. Heyler, D. Humm, J. Hutcheson, N. Izenberg, R. Lee, J. Lees, D. Lohr, E. Malaret, T. Martin, J.A. McGovern, P. McGuire, R. Morris, J. Mustard, S. Pelkey, E. Rhodes, M. Robinson, T. Roush, E. Schaefer, G. Seagrave, F. Seelos, P. Silverglate, S. Slavney, M. Smith, W.-J. Shyong, K. Strohbehn, H. Taylor, P. Thompson, B. Tossman, M. Wirzburger, and M. Wolff. 2007. CRISM (Compact Reconnaissance Imaging Spectrometer for Mars) on MRO (Mars Reconnaissance Orbiter). *Journal of Geophysical Research, 112*: E05S03.

Murchie, S., L. Roach, F. Seelos, R. Milliken, J. Mustard, R. Arvidson, J.-P. Bibring, J. Bishop, M. Parente, R. Morris, and J. Andrews-Hanna. 2008 submitted. Compositional evidence for the origin of layered deposits in Candor Chasma, Mars. *Nature*.

Nedell, S.S., S.W. Squyres, and D.W. Andersen. 1987. Origin and evolution of the layered deposits in the Valles Marineris, Mars. *Icarus, 70*: 409-441.

Okubo, C.H. and A.S. McEwen. 2007. Fracture-controlled paleo-fluid flow in Candor Chasma, Mars. *Science 315, 983; doi*: 10.1126/science.1136855.

Pelkey, S.M., J.F. Mustard, S. Murchie, R.T. Clancy, M. Wolff, M. Smith, R. Milliken, J.-P. Bibring, A. Gendrin, F. Poulet, Y. Langevin, and B. Gondet. 2007. CRISM multispectral summary products: Parameterizing mineral diversity on Mars from reflectance. *Journal of Geophysical Research, 112*: E08S14.

Peterson, C. 1981. A secondary origin for the Central Plateau of Hebes Chasma. *12th Lunar and Planetary Science Convention*, Part B, Pergamon Press, New York, 1459-1471.

Pondrelli, M., A. Pio Rossi, L. Marinangeli, E. Hauber, K. Gwinner, A. Baliva, and S. Di Lorenzo. 2008. Evolution and depositional environments of the Eberswalde fan delta, Mars. *Icarus 197*: 429–451.

Quantin, C., A. Gendrin, N. Mangold, J.-P. Bibring, E. Hauber, P Allemand and the OMEGA Team. 2006. Stratigraphy and elevation of sulfate deposits in Valles Marineris. *37th Lunar and Planetary Science Convention*, Abstract #2046.

Rossi, A.P., G. Neukum, M. Pondrelli, S. Van Gasselt, T. Zegers, E. Hauber, A. Chicarro, and B. Foing. 2008. Large-scale spring deposits on Mars? *Journal of Geophysical Research, 113(EO), 8016,* doi:10.1029/2007JE003062.

Schieber, J. 2007. Reinterpretation of the Martian Eberswalde Delta in the light of new HiRISE images. *38th Lunar and Planetary Science Convention*, Abstract #1982.

Schultz, R.A. and J. Lin. 2001. Three-dimensional normal faulting models of the Valles Marineris, Mars, and geodynamic implications. *Journal of Geophysical Research. 106 (B8)*: 16549-16566.

Schultz, R.A. 1998. Multiple-process origin of Valles Marineris basins and troughs, Mars. *Planetary Space Science, 46*: 827-834.

Smith, M.D., M.J. Wolff, R.T. Clancy, and S.L. Murchie. 2008 submitted. CRISM Observations of Water Vapor and Carbon Monoxide. *Journal of Geophysical Research.*

Weitz, C. M., R.E. Milliken, J.A. Grant, A.S. McEwen, R.M.E Williams and J.L. Bishop. 2008. Light toned strata and inverted channels adjacent to Juventae and Granges chasmata, Mars. *Geophysical Research Letters, Vol., 35 L19202, doi*: 10.1029/2008GL035317.

CHAPTER 4 – SOUTHERN ILD

Structural Analysis of an Interior Layered Deposits in Southern Coprates Chasma, Mars

H. Racher[a], F. Fueten[a], R. Stesky[b], P. MacKinnon[a], E. Hauber[c], T. Zegers[d], K. Gwinner[c].

[a]Department of Earth Sciences, Brock University, St. Catharines, Ontario, Canada L2S 3A1 < ffueten@brocku.ca>; [b]Pangaea Scientific, Brockville, Ontario, Canada; [c]Institute of Planetary Research, German Aerospace Center (DLR), Berlin, Germany; [d]Faculty of Geosciences, Utrecht University, Utrecht, The Netherlands.

ABSTRACT

A single interior layered deposit within the center of the southern portion of Coprates Chasma in Valles Marineris, Mars, is studied using HRSC, CTX, and HiRISE imaging. The outer limits are defined as a triangular shape with layering visible higher in the stratigraphic section along the sides and along the top of the mound. Dip directions mimic the direction of the local sloping topography. Apparent folding and fracturing along the triangular edge are observed, with fracture orientations being close to the Valles Marineris linear trend. An elongated mound situated against the tip of the triangular shaped mound appears to have a zone of deformation transecting directly through the center of the unusual deposit. The triangular deposit is interpreted as a large fault block back rotated 6° to the south and the small elongated mound is also a small fault block. It is suggested that the entire embayment around this deposit originated as a small ancestral basin. A displaced basement ridge is evidence of the early basin collapse to the north of this deposit. The central mound was most likely deposited and then tilted during the tectonism associated with the opening of the Valles Marineris. Following an erosion event, which coincided with or post-dated Valles Marineris formation, thin mesa covered most of the area.

INTRODUCTION

Interior layered deposits (ILDs) occur throughout the chasmata of the Valles Marineris. The layered deposits account for approximately 17% of the total area and 60% of all chasma deposits on Mars (Lucchitta *et al.*, 1994). The origin and mechanism of ILD formation is unknown and the theories are based on morphological and stratigraphic characteristics in different depositional environments. Several hypotheses are proposed, including lacustrine (Nedell *et al.*, 1987), aeolian (Peterson, 1981), pyroclastic volcanism in subaerial (Hynek *et al.*, 2003; Chapman, 2002; Lucchitta, 1987, 1990) or in subglacial (Nedell *et al.*, 1987; Chapman and Tanaka, 2001; Komatsu *et al.*, 2004) environments. Komatsu and Litasov (2002) propose the theory that the topography surrounding volcanic regions is comprised of successive layers of ash debris and account for the majority of the material within a layered deposit. Centralized vents within subglacial terrains may be capped with near horizontal layered deposits above the icy substrate. More recently it has been suggested that ILDs formed as spring deposits (Rossi *et al.*, 2008) and these deposits act as indicators of fluvial activity (Clarke and Bourke, 2009). Spring deposits are found in a wide range of scales and Clarke and Bourke (2009) suggest these deposits are unconformable to disconformable capped units from the resulting subsurface characteristics. All of these processes imply the troughs within which the ILDs formed existed prior to the formation of the ILDs. Malin and Edgett (2000) and Catling *et al.* (2006) suggest ILDs are ancient deposits buried beneath the material which form the walls of troughs. The diversity of ILD characteristics implies that several mechanisms were involved in their formation and all of which can provide an interpretation into past geological conditions.

The chasmata of Valles Marineris were likely formed during a two stage process (Lucchitta *et al.*, 1994; Schultz, 1998). Ancestral basins which are isolated depressions with irregular outlines were proposed to have formed prior to the opening of the Valles Marineris during rift-like faulting (Lucchitta and Bertolini, 1990; Lucchitta *et al.*, 1994). Lucchitta *et al.* (1994) suggested that Hebes, south Ophir, south Candor and potentially south Melas Chasma were sites of ancestral basins. It is noted, much of Coprates, north Melas and Ius may have formed during the later faulting episodes (Lucchitta *et al.*, 1994). Closed depressions appear to have no lateral removal of material and require a downward displacement, a collapse of material into a pre-existing void (Shultz, 1997). Whereas the chasmata that formed later with tectonism have rectangular troughs consistent with the mechanism yet; faulting cannot account for all the irregular outlines of the basins (Shultz, 1997). Faulting resulting from the opening of the Valles Marineris (Schultz, 1998) connected surrounding basins and forming the current rift valley configuration.

A recent model for ILD formation, based on stratigraphic and structural observations (Fueten *et al.*, 2008) within western Candor Chasma suggests that deposition occurred synchronously with subsidence of early basins and that individual subsiding basin blocks may be identified. According to this model the deposition takes place without the formation of obvious unconformities or disconformities during the subsidence phase, but was followed by a major period of erosion, most likely associated with the linkage of basins and the establishment of drainage channels during the opening of Valles Marineris. Following that period of erosion, there is evidence for only minor deposition.

In this study, the general methodology of Fueten *et al.* (2008) is followed to study

a layered deposit located within Coprates Chasma to test the proposed model.

Geological Setting

The study area in the south of Coprates Chasma contains one large interior layered deposit and a smaller elongated mound. The peak of the larger deposit is approximately 2 km higher in elevation than the canyon floor which is 8 km deep and is located between wall rock to the north east and south (Fig. 4-1A). The larger layered deposit is roughly triangular with XYZ defined as the outer corners (Fig. 4-1B). The elongated mound is located immediately north of Y. The ILD is approximately 35 km long from X-Z (blue arrow) and 17 km wide (red arrow) from the northern tip of the elongated mound to the mid point on the top of the main mound (Fig. 4-1B). The difference in elevation from X to Y is approximately 1 km indicating that, the western limits of the triangular edge are tilted (Fig. 4-1C). The elongated mound appears to contain no clearly identifiable layering along the surface and is 3.5 km wide and 6.5 km long with an elevation of 1.5 km above the chasma floor. However, visible layering is identified along the triangular edge and on the top of the main mound.

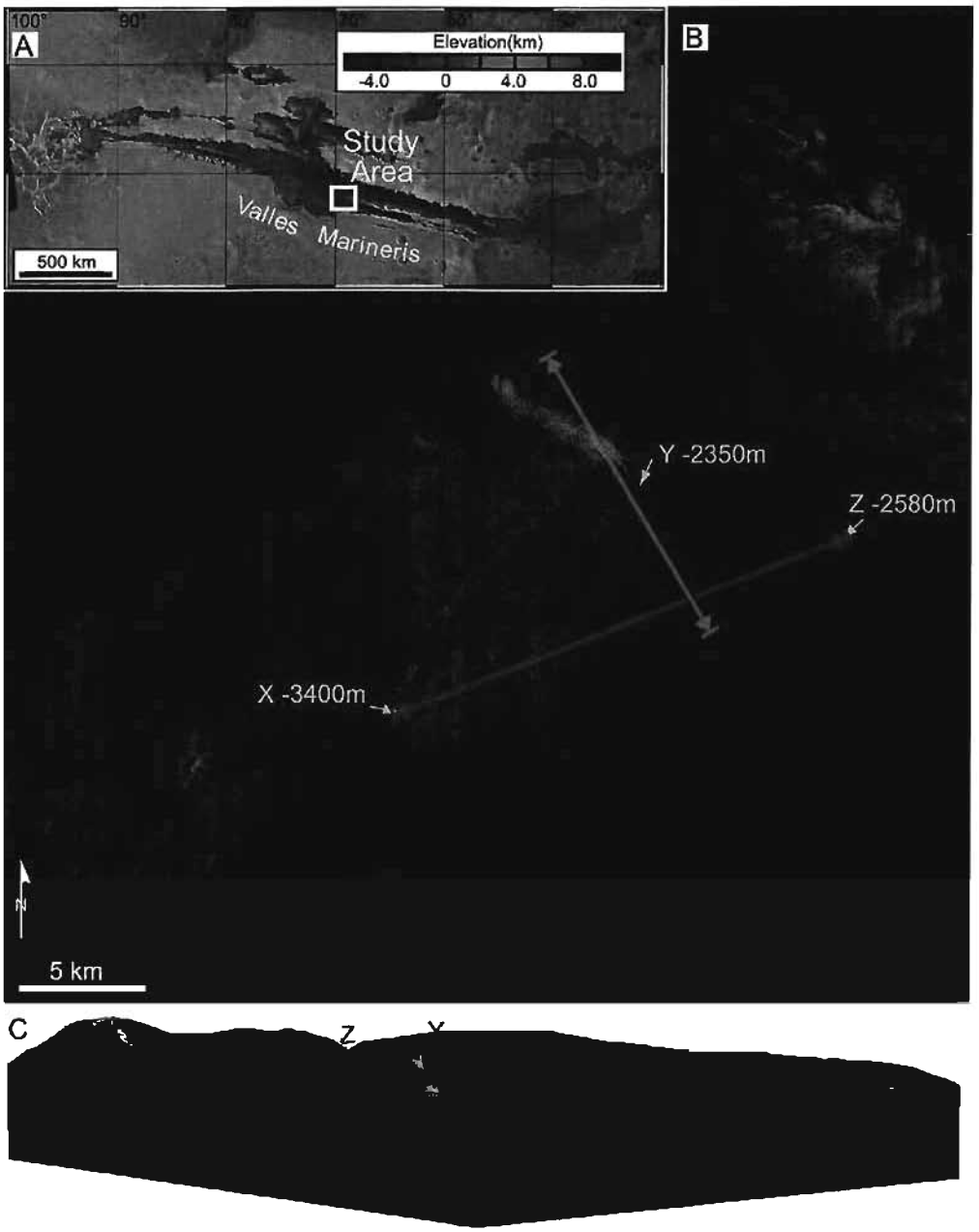

Figure 4-1. Inset A: Location of triangular edged ILD and elongated shaped mound in southern Coprates Chasma. Inset B: HRSC image with the DEM show the western limits indicated as X to Y and the eastern limits indicated as Y to Z that mark the boundary of the layered deposit. The red arrow marks the measured width of the deposit and the blue arrow marks the measured length. Inset C: 3D image of triangular limits of main mound with no vertical exaggeration. (Racher *et al.*, 2009)

Methodology for Attitude Measurements

A High Resolution Stereo Camera (HRSC; Jaumann *et al.*, 2007) panchromatic orthoimages were obtained during the orbit 2039 with a resolution of 12.5 m/pixel. The HRSC images have a corresponding Digital Elevation Model (DEM) with a grid spacing of 50 m. The HRSC images form the primary data set of the study. Three context images for southern Coprates Chasma (CTX; Malin *et al.*, 2007) (P01_001522_1677_XN_12S069W_CTX, P08_004054_1688_XI_11S069W_CTX, P13_005966_1685_XI_11S069W_CTX) with a resolution of 6 m/pixel were manually registered to the HRSC image by coordinate referencing using Global Mapper Software. Layering attitudes were measured on both the HRSC image and the CTX composite using ORION software. The methodology is discussed in detail by Fueten *et al.* (2005). ORION is used to plot points along an obvious plane and possible stratigraphic layer, where the strike, dip, maximum deviation and percent accuracy are measured. Layers that could be clearly identified in both HRSC and CTX images, the measurements were in good agreement as is illustrated in Table 4-1. HiRISE (High Resolution Imaging Science Experiment at 25 m/pixel; McEwen *et al.*, 2007) image for the south which primarily covers the elongated mound (PSP_004054_1675) of Coprates Chasma was also used for observations but not registered to the DEM due to the large difference in the horizontal scale.

	HRSC		CTX		HRSC			CTX		
	Strike	Dip	Strike	Dip	# of points	Trace Length (m)	Max. deviation (m)	# of points	Trace Length (m)	Max. deviation (m)
X	45.7 ± 22.2	3.8 ± 1.5	95.2 ± 33.9	1.9 ± 1.4	11	975	0.51	17	5319	5.39
	263.0 ± 3.5	7.6 ± 2.0	261.3 ± 6.1	5.5 ± 2.0	9	1133	0.21	16	1879	0.92
Y	103.5 ± 10.4	4.6 ± 2.0	97.7 ± 9.8	4.7 ± 1.7	46	2433	4.31	19	4049	5.87
	136.5 ± 23.8	4.5 ± 1.8	100.1 ± 7.1	6.3 ± 1.8	9	1745	2.65	9	1372	1.22
Z	179.6 ± 48.2	2.5 ± 1.3	258.0 ± 33.2	1.4 ± 1.8	11	1374	0.55	15	3005	2.01
	293.5 ± 3.8	12.3 ± 1.8	284.1 ± 3.3	8.4 ± 1.7	15	1954	0.55	11	1617	0.38

Table 4-1. Comparison of attitude for layers measured within both, HRSC and CTX mosaic images of southern Coprates Chasma. Measurements from all three elevation locations are presented. All planes have correlation coefficients greater than 0.99789.

OBSERVATIONS

Main Mound

The main triangular shaped mound is approximately 110 km south of the northern ILDs which were investigated by Fueten *et al.* (2009) and 30 km from the southern most wall rock in Coprates Chasma. The northern edge (Y-Z) of the triangular deposit appears to plunge in the direction of the local slope, south east at approximately 5° and on the western edge (X-Y) plunges towards south west at approximately 6°. Layering is visible only in the higher stratigraphic sections; layering extends 150 m below the top surface of the mound along the X-Y and 300 m along Y-Z edges. It is assumed that layering extends to the base of the deposit however; it is not visible due to the accumulation of debris.

The layering attitudes within the main triangular mound vary with location and stratigraphic position. Layering is traced for longer distances along the X-Y and Y-Z boundaries and layering is also found to dip more steeply than along the top of the mound. Layering can be traced for distances of 10 km along the X-Y section with a westerly dip direction which mimics the local topography. The dip values recorded range between 2° and 11° however, closer to location X the layering is essentially horizontal (Fig. 4-2A). Layering along Y-Z mimics the local topography with a dip direction to the south west and layering near location Z appears to be horizontal (Fig. 4-2B). Layering on the top of the mound can only be traced for approximately 5 km. Layers near Y have dip values ranging from 5° to 6° dipping to the south (Fig. 4-2A). Farther away from the edges on the top of the main mound dip values are recorded around 5° (Fig. 4-2A). The base of the mound from X-Y and Y-Z is primarily covered by thin mesa material which

impedes any layering measurements (Fig. 4-2C). Even more thin mesa material is found farther up the stratigraphic section, to the west of the X-Y triangular edge on the top of the main mound and the material obstructs the visible presence of layering.

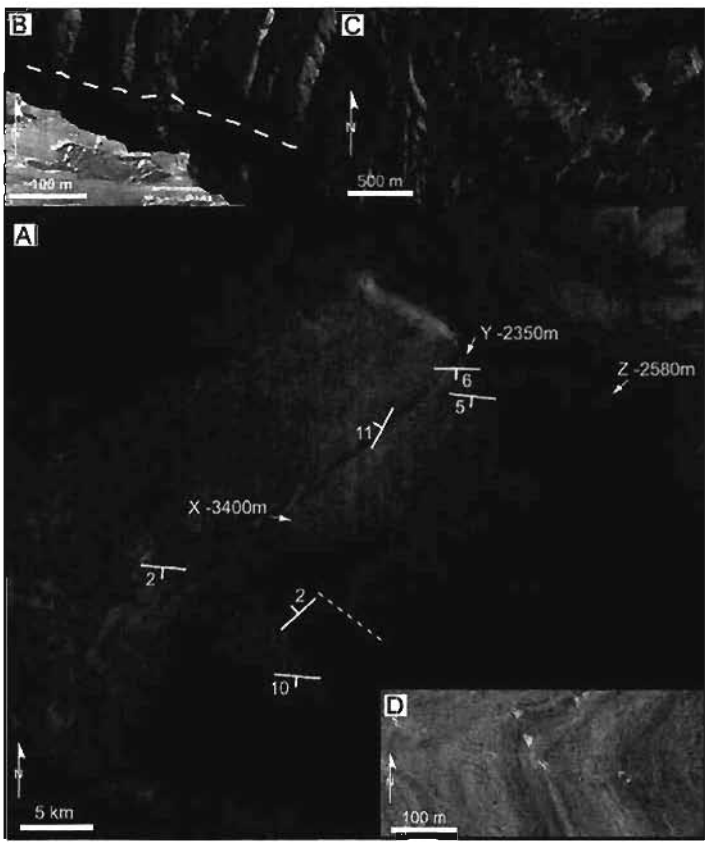

Figure 4-2. Inset A: HRSC image of triangular edge mound and elongated shaped mound with associated dip values at X, Y, Z locations and of various traceable layers higher in the stratigraphic section. Inset B: Layering observed in the HiRISE image, PSP_004054_1675 at location Z is nearly horizontal (white dashed line). Inset C: CTX mosaic (P01_001522_1677_XN_12S069W_CTX, P08_004054_1688_XI_11S069W_CTX, P13_005966_1685_XI_11S069W_CTX) showing thin mesa covering much of the wall rock. Black arrows indicate part of the boundary of thin mesa material. Inset D: HiRISE image, PSP_004054_1675 shows the banded light and dark lithologies of layering on the top of the main mound.

Layering observed in the HiRISE image PSP_004054_1675 on top of the main mound appears as light and dark lithologies (Fig. 4-2D). Using the horizontal width of the layers displayed within the HiRISE image and the inclination of the local slope on the top of the mound from the HRSC DEM, the layering thickness is estimated. The dark layers have a thickness range from approximately 5 m to 60 m. The lighter layers appear to be thinner than the darker lithology with a thickness range from 2 m to 30 m.

A north west to south east trending break transects the main ILD mound in both HRSC and CTX images. There is an elevation drop of approximately 50 m along the north east side of the break (Fig. 4-3). The visible extent of the break is approximately 4.5 km in length. There is an elevation drop of approximately 115 m along the north west flank which covers the entire extent of visible layering and a 300 m elevation drop along the south west side. Thin mesa material is visible to the north west and south east of this separate layered deposit. The thin mesa appears to obstruct the further extent of layering to the north west and possibly the continuing extent of the transecting break towards the triangular edge.

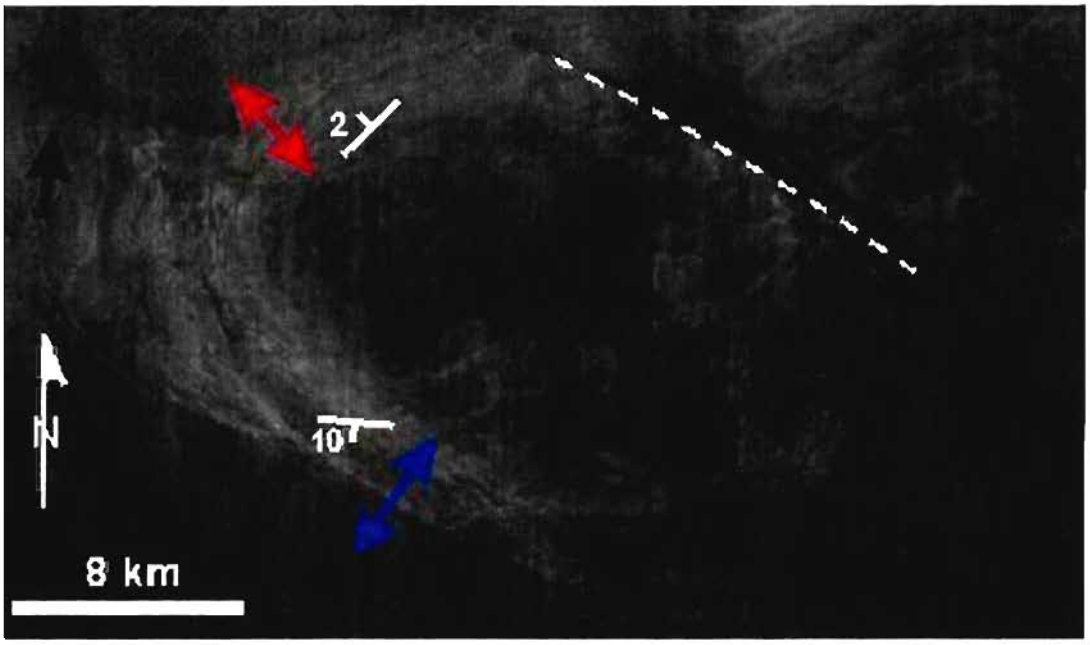

Figure 4-3. A north east to south east trending break transects the main mound observed within the CTX image, P08_004054_1668_XI_ 11S069W with an elevation drop in 50 m to the north east (white dashed line). The elevation drop along the north west flank is marked by a red arrow and the south west elevation drop is marked by a blue arrow. Black arrows indicate thin mesa locations.

Layering on top of the mound has a folded appearance. Numerous apparent folds are visible towards the center of the main mound (Fig. 4-4A). The apparent folds range in amplitude from 50 m to 200 m and also range in width from 50 m to 100 m. At several locations however, layering appears to be truncated by folding (Fig. 4-4B). The truncations cut off the adjacent layering. Minor offsetting of layering is visible in Figure 4-4C but in most cases no major offsets are observed.

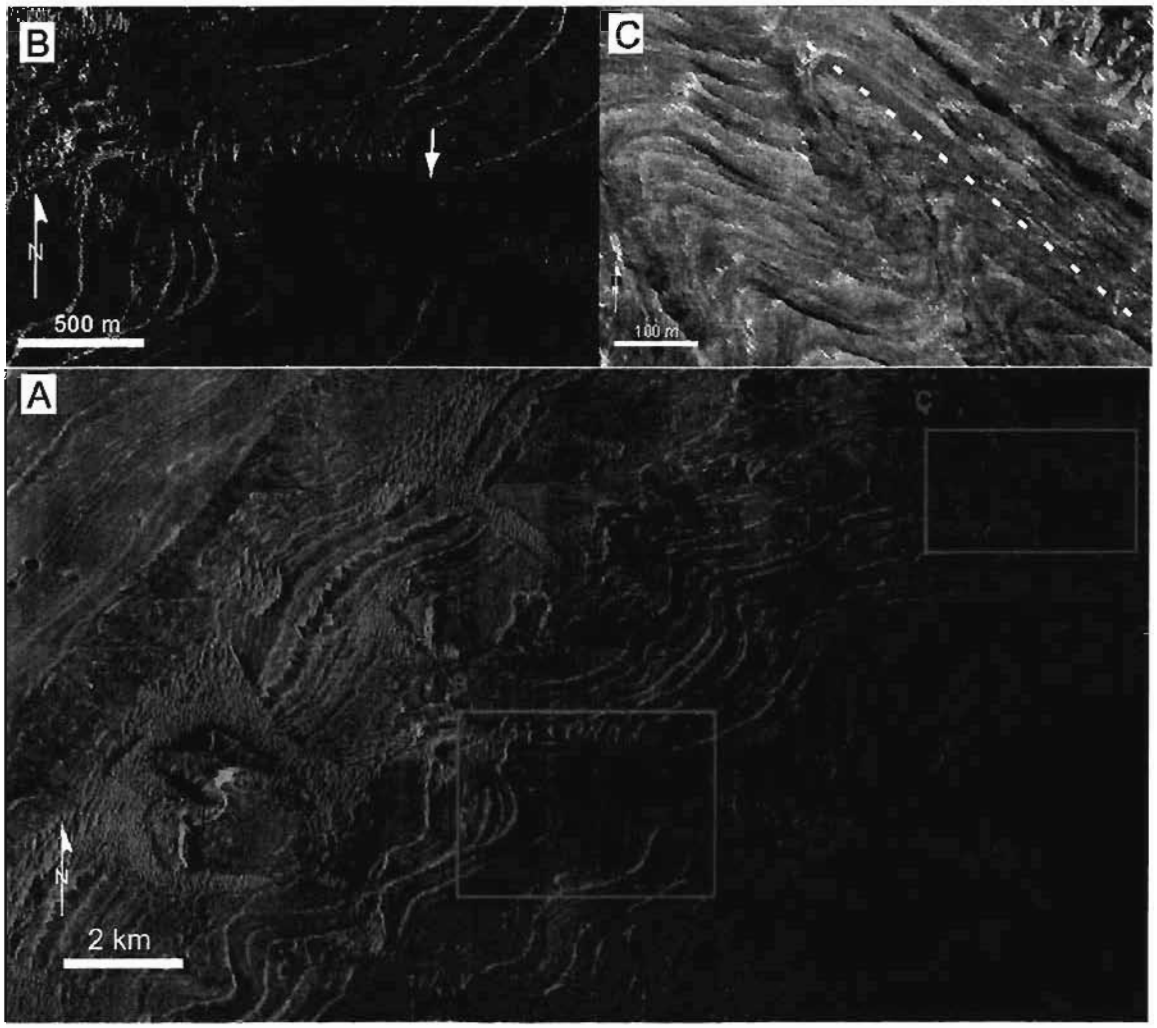

Figure 4-4. Inset A: CTX mosaic (P01_001522_1677_XN_12S069W_CTX, P08_004054_1688_XI_11S069W_CTX, P13_005966_1685_XI_11S069W_CTX). Location map of truncations and apparent folding on the top of the main mound. Inset B: the location of the truncation (white arrow) in the HiRISE image, PSP_004054_1675. Inset C: the location of the steep fold (white line indicates the disruption of layering) in HiRISE image, PSP_004054_1675.

Also visible in the HiRISE image, are fracture sets (Fig. 4-5A, Table 4-2). These fractures are commonly found along the X-Y edge trending in an east to west direction

(Fig. 4-5A). It is also observed two fracture sets occur with an east to west and a north west to south east orientation. The north west to south east fracture set is more dominant with longer fractures cutting across smaller, less visible east to west fractures (Fig. 4-6B). Layering is not significantly offset by any fracturing or faulting along the triangular edge (Fig. 4-6C). Along the X-Y and Y-Z edges, more variation in fracture trend is observed compared to those fractures found farther away from the edge. Closer to location Y, the fractures are oriented in a north east, south west direction. Primarily, the overall trend of the observed fractures either along the triangular edge or farther on the main mound is 090°. These fractures appear similar to those presented by Okubo and McEwen (2007) that are related to fluid alteration within the subsurface. There is no major offset of layering as a result of this fracturing and faulting (Fig. 4-6D). Wyrick *et al.* (2005) associates similar normal faults to the interconnectedness of fault networks or isolated fault blocks. It is suggested the formation of the faults results from tectonism and fluid movement through a faulted aquifer (Wyrick *et al.*, 2005).

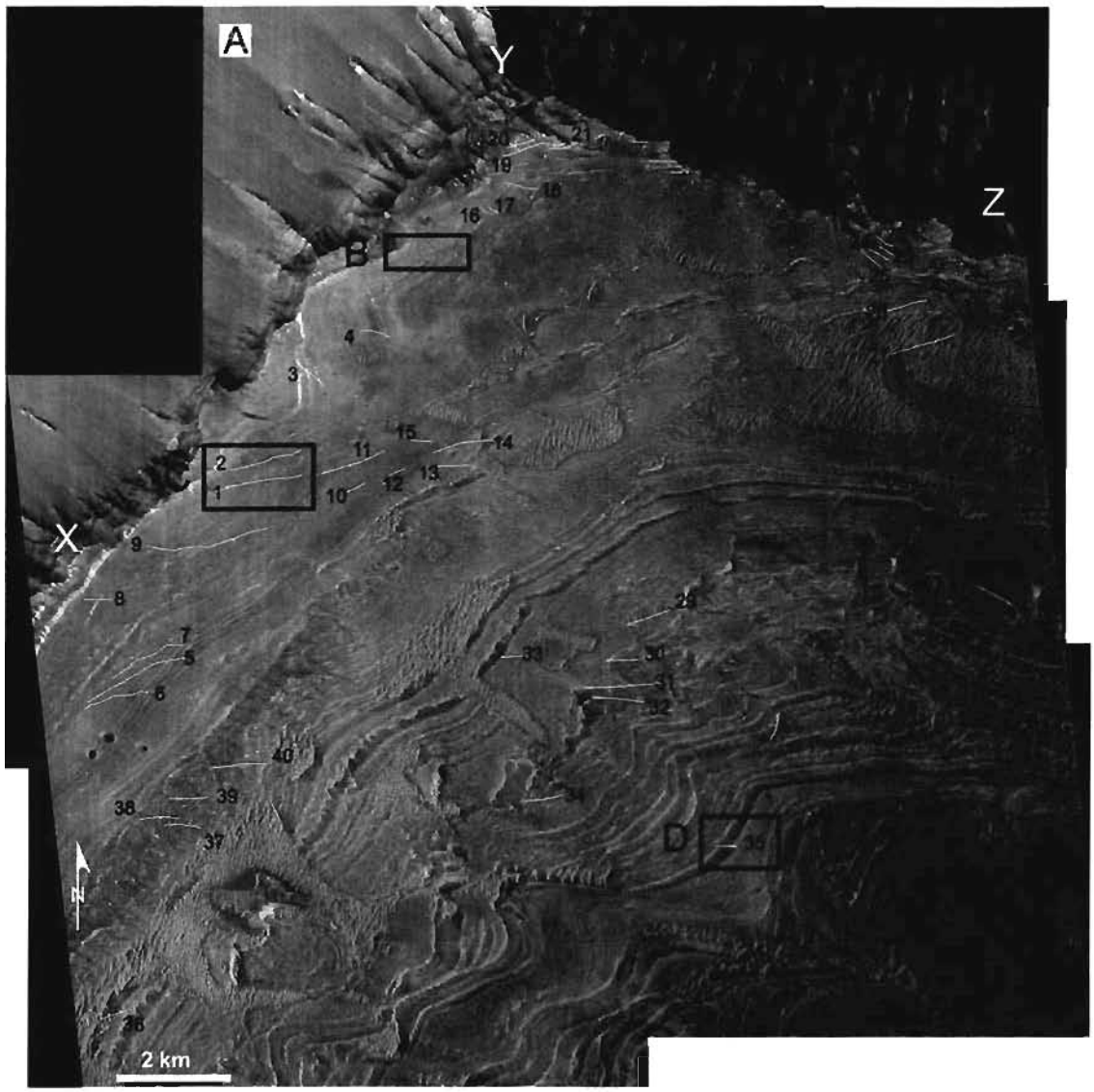

Figure 4-5. CTX mosaic (P01_001522_1677_XN_12S069W_CTX, P08_004054_1688_XI_11S069W_CTX, P13_005966_1685_XI_11S069W_CTX) indicates the overall orientation of fractures found along the top of the mound. Each fracture is numbered with corresponding statistics (refer to Table 4-2). For insets B, C and D refer to Figure 4-5.

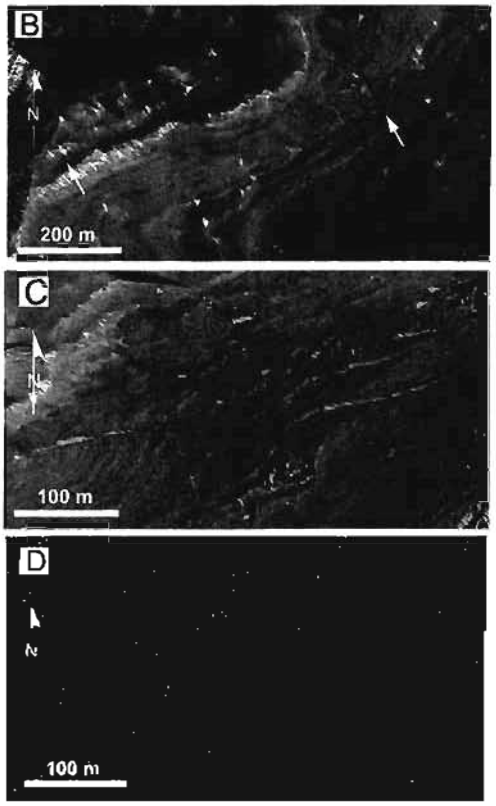

Figure 4-6. Inset B: Fracture sets (arrows) are observed in the HiRISE image, PSP_004054_1675 near edge of the ILD. Inset C: Fractures trending east to west on top of main mound observed in HiRISE image PSP_004054_1675. Inset D: Slight offset of layering by an east to west trending fault observed in HiRISE image PSP_004054_1675 along the top of the main mound. Location shown within Figure 4-5.

Number	Length (m)	Trend (°)	Near Location
1	764	72	XY
2	630	80	XY
3	230	123	XY
4	200	125	XY
5	800	66	XY
6	750	69	XY
7	775	64	XY
8	270	100	XY
9	850	81	XY
10	200	70	XY
11	700	76	XY
12	190	77	XY
13	270	89	XY
14	450	90	XY
15	120	84	XY
16	110	102	XY
17	150	104	XY
18	350	105	Y
19	300	72	Y
20	225	72	Y
21	200	61	Y
22	85	116	YZ
23	70	123	YZ
24	75	125	YZ
25	100	125	YZ
26	300	78	YZ
27	450	79	YZ
28	350	123	CENTRAL
29	320	77	CENTRAL
30	195	90	CENTRAL
31	550	88	CENTRAL
32	510	86	CENTRAL
33	175	86	CENTRAL
34	220	75	CENTRAL
35	150	100	CENTRAL
36	200	90	CENTRAL
37	215	88	CENTRAL
38	230	89	CENTRAL
39	230	90	CENTRAL
40	600	90	CENTRAL

Table 4-2. Corresponding measurements and orientations for the observed fractures in the CTX mosaic (P01_001522_1677_XN_12S069W_CTX, P08_004054_1688_XI_11S069W_CTX, P13_005966_1685_XI_11S069W_CTX). The general trend observed was from an east to west orientation once the fractures were measured from the Y to Z section and further centered on the mound.

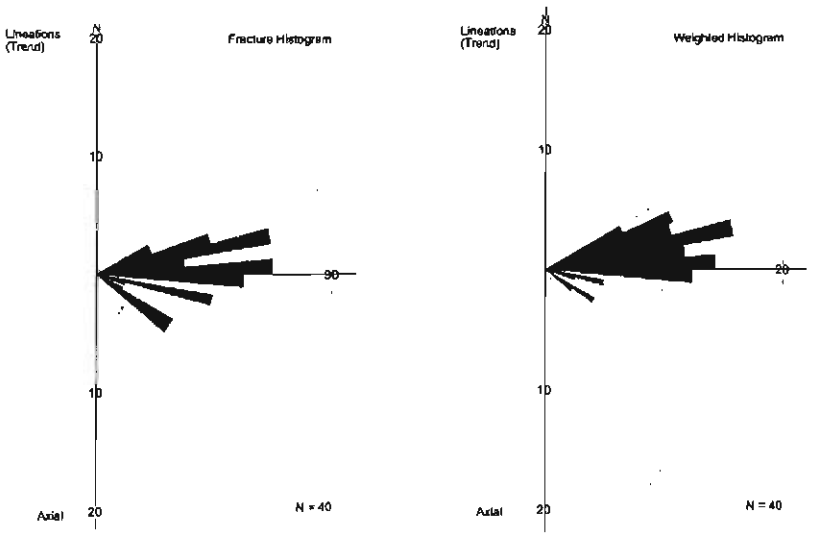

Table 4-3. The histogram measured in percent was plotted using the statistics from the 40 fracture sets viewed in Table 4-2. Histogram A: The frequency distribution of the trend statistics. The highest frequency is between 85° to 95°. Histogram B: Data weighted by length. This data indicates the longer and arguably more significant fractures trend between 85° and 90°.

Elongated Deposit

The elongated shaped deposit is situated adjacent to location Y of the main triangular mound oriented in a north westerly to south easterly direction. The elongated deposit is approximately 550 m below the elevation of the northern tip the main mound (Y). The deposit is 3.5 km wide, 6.5 km long and 1.5 km high in the entire extent. There is an obvious north west to south east planar scarp that forms the western side of the deposit and is approximately 4.7 km in length (Fig. 4-7A). This planar scarp can not be traced into the main mound or past the northern limits of the elongated deposit. The planar scarp has an orientation of 126°/35°; the topography of the eastern side of the mound is an irregular curved surface (Fig. 4-7C). No convincing layering is observed

along the elongated mound in the CTX, HiRISE or HRSC images. There is light and dark banding present on the elongated mound to the east of the central break. The banding has an appearance of a layered sequence however, layer traces cannot be measured with any accuracy in the CTX, HiRISE or HRSC images.

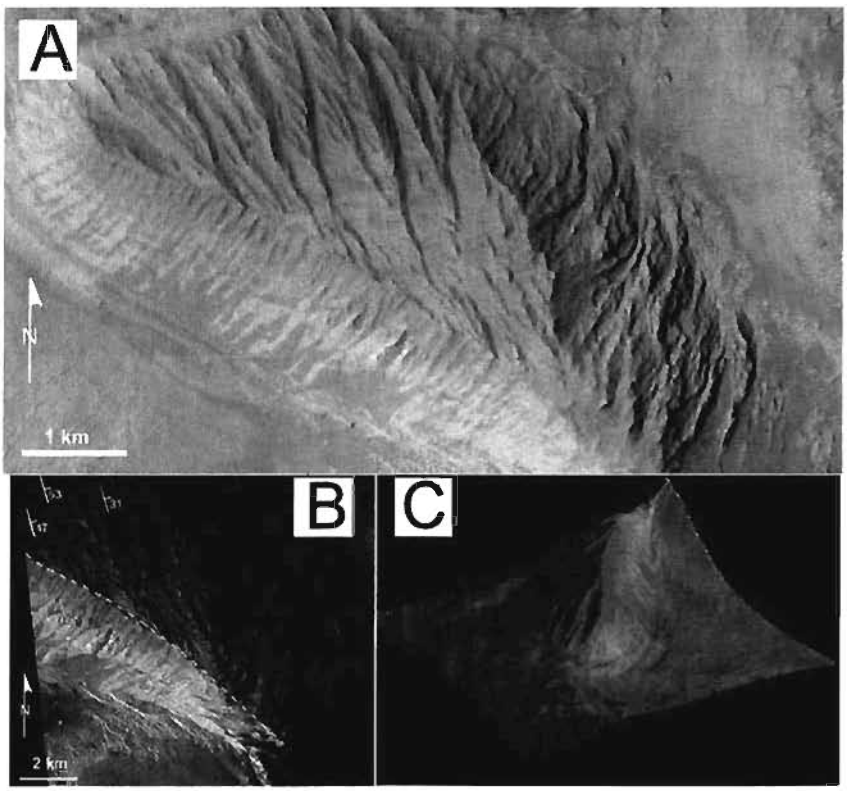

Figure 4-7. Inset A: Image from CTX mosaic, P01_001522_1677_XN_12S069W_CTX, P08_004054_1688_XI_11S069W_CTX, P13_005966_1685_XI_11S069W_CTX. Inset B: Elongated mound observed in HiRISE image PSP_004054_1675, the north western tip is not visible. The yellow dashed line is the fault scarp. The dip values are measured along possible fault scarps that are trending in a north west to south east direction. Inset C: The 3D profile of the HRSC image depicts the unusual topography of the elongated mound. In this image, to the west the slope is planar and steep, to the east the slope is gradually declining.

A series of ridges are observed to the east of the transecting break on the elongated mound. These ridges follow a north west to south east orientation (Fig. 4-8). The ridges do not appear to be eroded layers. The ridges are asymmetrical, with planar scarps dipping to the east and more irregular western slopes. The planar scarps have a dip values ranging between 30° and 50° to the north east (Fig. 4-7B). These scarps are interpreted as large planar fractures or possibly faults, in which no visible layering offset can be detected.

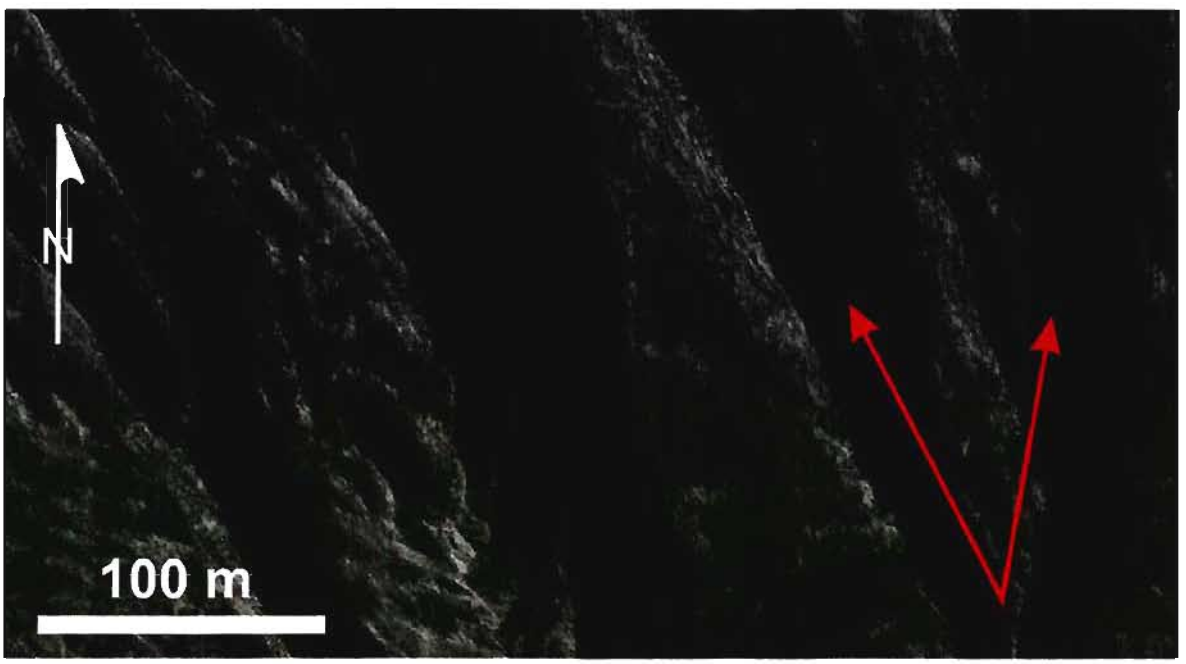

Figure 4-8. Ridges with planar scarps dipping to the east (red arrows) slightly perpendicular to the transecting break observed in HiRISE image PSP_004054_1675.

The large planar scarp on the west of the elongated mound does not have any linear ridges and no layering is visible (Fig. 4-9A). The surface appears to be highly eroded and heavily fractured. The fractured material ranges in size from 5 m to 30 m (Fig. 4-9B). This planar scarp is interpreted as a fault. The darker material is

accumulated in debris piles at the base of the slope (Fig. 4-9C). The small landslide scars appear to begin along the transecting break and flow downwards leaving an apron of debris at the bottom of the slope. The width size of the debris fan ranges from 100 m to 200 m and the length varies between 2 km, closer to the northern tip and 900 m closer to the main mound. The debris fans appear to be the result of erosion of the fault.

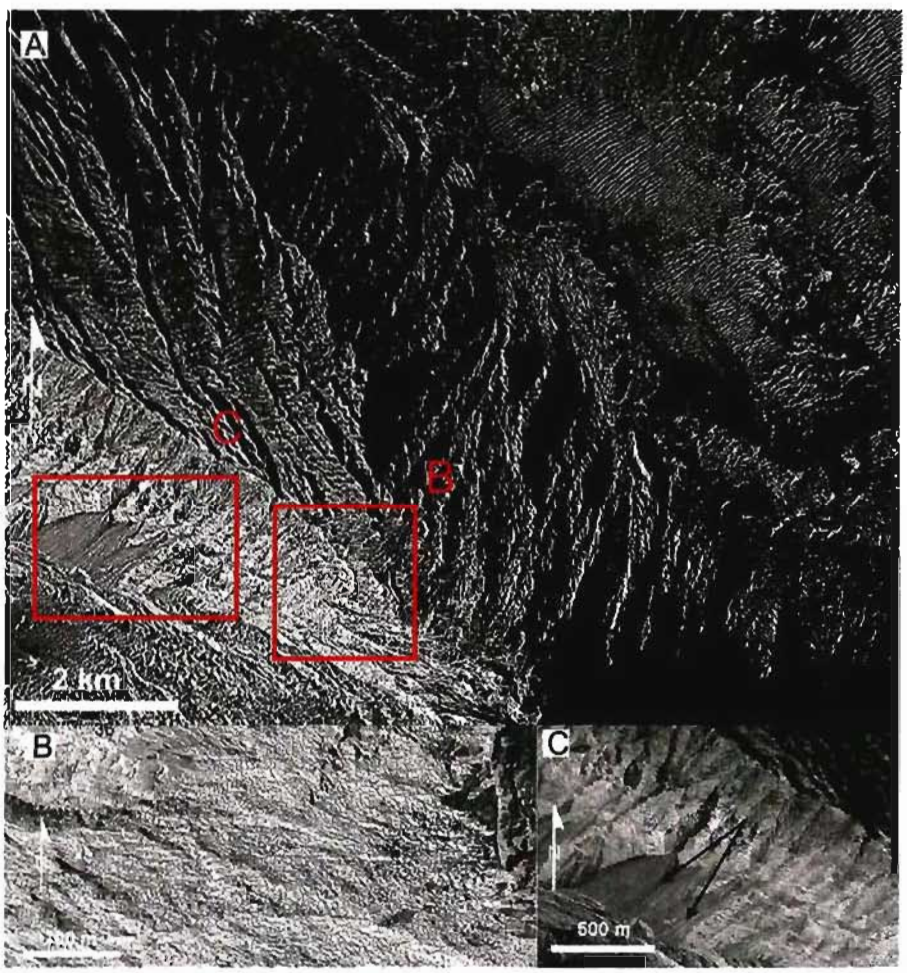

Figure 4-9. Inset A: HiRISE image PSP_004054_1675 of elongated mound indicating the locations of various erosional features to the west of the fault. Inset B: Heavily fractured material seen in the HiRISE image PSP_004054_1675. Inset C: Small debris fans (black arrows) located at the base of the steep slope to the west of the transecting fault and observed in the HiRISE image PSP_004054_1675.

DISCUSSION

Main Mound

The main mound is a single fault block which has undergone rotation. The northern limits of the block are defined by the scarp along XYZ. The approximate axis of rotation is suggested to be horizontal, trending approximately east to west. Looking towards the east, a clockwise rotation would produce the observed geometry of Y as the highest point, Z as the intermediate and X the lowest. Layering near Y dips approximately 6° and is approximately parallel to the overall topography, hence it is suggested that the amount of rotation was approximately 6°.

The predominant east to west fracture orientation would be consistent with fractures produced by rotation about an east to west axis. Variations in fracture orientations, such as the north to south fractures near the edges may simply reflect variation in local stress near the edge of the fault block. However, it should be pointed out that the fractures trending in an east to west direction are also close to the overall trend of the Valles Marineris. The southern wall rock is parallel to the orientation of the east to west fractures. The fractures were likely caused by the opening and associated tectonism of the Valles Marineris.

An obvious structural break in geology transects the top of the main mound in a north west to south east direction. Racher *et al.* (2009) proposed that the break transecting the ILD has elevation drop of 50 m to the north east. Layering along the triangular edge to the west of this break appears to be nearly horizontal. Hence, it is suggested that this break is a minor fault which forms the approximate southern boundary of the rotated block.

The truncations and folded appearance of layering on the main mound are consistent with shallow angular unconformities as suggested by Racher *et al.* (2009). It is suggested that layers were originally deposited horizontally and then rotated during tilting. Subsequent deposition of further layering upon a tilted substrate would produce shallow angular unconformities. Erosion of a package of layered material with such unconformities would produce the truncations observed. The apparent folds are a topographic effect, produced by a gently undulating erosional surface.

These observations of the fault block fit within the framework that the formation of Coprates Chasma coinciding with the tectonism of the opening and widening of the Valles Marineris (Schultz and Lin, 2001). The tectonism associated with a large rift valley would cause displacement within the underlying crust which in turn would create such a fault block. The tilt of the fault block exposes a scarp along the triangular edges. The elevated fault block can be interpreted as a horst and the surrounding lowered topography as the graben; structures associated with the formation of a rift valley.

Thin mesa covers most of the main mound affecting the accuracy of layering measurements primarily along the top of the mound. The thin mesa in this region shows signs of erosion. The thin mesa observed in southern Coprates Chasma is primarily preserved along slopes of the triangular edges and the surrounding flat regions of the fault block. Along the top of the triangular mound erosion has affected the uniform thin mesa coverage as lighter layering is visible especially closer to the edge. Farther inward on the fault block, the thin mesa coverage appears to heavily blanket the surface. The lack of thin mesa material at higher elevations particularly around location Y but also along the triangular edge, suggests this topography is exposed to more active wind erosion. As

mentioned previously, lower in the stratigraphic section of the triangular edge there is thin mesa coverage. This suggests the overall geometry of the main mound has not been significantly modified since the last thin mesa depositional event.

Elongated Deposit

The elongated deposit, north west of location Y is suggested to be a remnant of material north of the fault. Several east dipping fracture scarps occur along the top surface. Layering on this deposit can not be traced with confidence, most likely because of the fracturing. A fault, 4.7 km long, trending north west to south east forms the western edge of the mound. There is no evidence that this fault extends into the main mound. It is proposed this elongated mound was deposited as possibly a part of the same stratigraphic package as the main mound and was deformed and moved into its current position during the rotation of the fault block. The top of the elongated mound is situated 550 m lower than location Y of the main mound and would suggest this is a separate fault block displaced through tectonism from the main mound. The break in elevation between the two mounds was likely caused by the rotation of the main mound. The minimal coverage of thin mesa seen to the western side of the fault suggests erosion or deformation of the surface has occurred recently, post-dating thin mesa deposition. However, thin mesa also covers the surface to the east of the break which suggests that the elongated deposit has not been significantly modified since the last depositional event.

Timing of Deformation

The fault block may have formed during the opening of the Valles Marineris which was then further back rotated during the associated tectonism creating the triangular edge. It has been suggested that the opening of the Valles Marineris led to the major depositional and erosional events observed within Coprates Chasma (Fueten *et al.*, 2008). Observations obtained for southern Coprates Chasma are agreeable with the timing of this erosional and depositional model. Erosion along the top of the fault block exposed the underlying layers. The ILD observed within southern Coprates Chasma appear to have been present prior to the opening of the Valles Marineris. However, deposition of layered material must still have taken place during the rotation of the fault block as the resulting unconformities were observed. Coprates Chasma existed or was in the process of forming when the major erosional event occurred. The thin mesa would have been a depositional episode after the major erosional event. The thin mesa evenly covers much of southern Coprates Chasma and appears to have undergone no deformation and only minor erosion, the deposition of the thin mesa material represents the latest event.

CONCLUSION

The fault block rotation is consistent with the opening of a rift valley such as the opening of the Valles Marineris. The layered deposit formed and then was exposed to further deformation from the faulting associated with the opening of the rift valley. The ILD is situated to the south west of the wall rock and is concluded to post-date the deposition of the basement rock. The mode of deposition is not determined for the ILD in southern Coprates Chasma. Mineralogical data is not available for this region of Coprates Chasma. During the formation of the Valles Marineris, the fault block and elongated mound achieved the present configuration. The associated tectonism of the Valles Marineris displaced the elongated mound from the fault block as the block experienced back rotation. Continued movement along the fault block further separated the elongated mound from the main deposit. The fault along the long axis of the elongated deposit was most likely the result of tilting and uplifting. The thin mesa deposit appeared to have been deposited as a regionally extensive blanket which has been partially eroded especially on the top of the fault block since deposition. The thin mesa covers most of the wall slope and is concluded that the wall rock has not been significantly eroded since the last depositional period.

ACKNOWLEDGEMENTS

We thank the HRSC Experiment Teams at DLR Berlin and Freie Universitaet Berlin, and the Mars Express Project Teams at ESTEC and ESOC for their successful planning and acquisition of data, as well as for making the processed data available to the HRSC Team. We also want to thank the CTX and HiRISE Teams for making their data available. This project was partially funded by an NSERC discovery grant to F. Fueten. Pangaea Scientific thanks P. Budkewitsch and Canada Centre for Remote Sensing for support of ORION under contract NRCan-01-0102.

REFERENCES

Catling, D.C., S.E. Wood, C. Leovy, D.R. Montgomery, H.M. Greenberg, C.R. Glein, J.M. Moore. 2006. Light-toned layered deposits in Juventae Chasma, Mars. *Icarus, 181*: 26-51.

Chapman, M.G. 2002. Layered, massive, and thin sediments on Mars: Possible Late Noachian to Late Amazonian tephra? In: Smellie, J.L. and M.G. Chapman, (eds). Volcano-Ice Interactions on Earth and Mars. *Geological Society, London, Special Publications, 202*: 273-203.

Chapman, M.G., and K.L. Tanaka. 2001. Interior trough deposits on Mars: Subice volcanoes? *Journal of Geophysical Research, 106(E5)*: 10,087-10,100.

Fueten, F., R. Stesky, P. MacKinnon, E. Hauber, T. Zegers, K. Gwinner, F. Scholten, and G. Neukum. 2008. Stratigraphy and structure of interior layered deposits in west Candor Chasma, Mars, from High Resolution Stereo Camera (HRSC) stereo imagery and derived elevations. *Journal of Geophysical Research, 113, E10008, doi:*10.1029/2007JE003053.

Fueten, F., R.M. Stesky, and P. MacKinnon. 2005. Structural attitudes of large scale layering in Valles Marineris, Mars, calculated from Mars Orbiter Laser Altimeter data and Mars Orbiter Camera imagery. *Icarus, 175*: Issue 1, 68-77.

Hauber, E., K. Gwinner, A. Gendrin, F. Fueten, R. Stesky, S. Pelkey, H. Wulf, D. Reiss, T. Zegers, P. MacKinnon, G. Michael, R. Jaumann, J.-P. Bibring, G. Neukum, and the HRSC Co-Investigator Team. 2006. An integrated study of interior layered deposits in Hebes Chasma, Valles Marineris, Mars, using MGS, MO, and MEX Data. *37th Lunar and Planetary Science Convention*, Abstract #2022.

Hynek, B.M., R.J. Phillips, and R.E. Arvidson. 2003. Explosive volcanism in the Tharsis region: Global evidence in the Martian record. *Journal of Geophysical Research, 108(E9), 5111, doi*: 10.1029/2003JE002062.

Jaumann, R., G. Neukum, T. Behnke, T. Duxbury, K. Eichentopf, J Flohrer, S. Gasselt, B. Giese, K. Gwinner, E. Hauber, H. Hoffmann, A. Hoffmeister, U. Köhler, K. Matz, T. McCord, V. Mertens, J. Oberst, R. Pischel, D. Reiss, E. Ress, T. Roatsch, P. Saiger, Scholten, G. Schwarz, K. Stephan, M. Wählisch, and the HRSC Co-Investigator Team. 2007. The high-resolution stereo camera (HRSC) experiment on Mars Express: Instrument aspects and experiment conduct from interplanetary cruise through the nominal mission. *Planetary Space Science, 55*: 928-952.

Komatsu, G., G.G. Ori, P. Ciarcelluti, and Y.D. Litasov. 2004. Interior layered deposits of Valles Marineris, Mars: analogous subice volcanism related to Baikal Rifting, Southern Siberia. *Planetary Space Science, 52*: 167-187.

Komatsu, G., P.E. Geissler, R.G. Strom, and R.B Singer. 1993. Stratigraphy and erosional landforms of layered deposits in Valles Marineris, Mars. *Journal of Geophysical Research, 98*: 11,105–11,121.

Lucchitta, B.K., N.K. Isbell, and A. Howington-Kraus. 1994. Topography of Valles Marineris: Implications for erosional and structural history. *Journal of Geophysical Research, 99*: 3783-3798.

Lucchitta, B.K. 1990. Young volcanic deposits in the Valles Marineris, Mars? *Icarus, 86*: 476-509.

Lucchitta, B.K and M.L. Bertolini. 1990. Interior structures of Valles Marineris, Mars. *20th Lunar and Planetary Science Convention*, Abstract #590-591.

Lucchitta, B.K. 1987. Recent mafic volcanism on Mars. *Science, 235*: 565-567.

Malin, M.C., J. Bell, B. Cantor, M. Caplinger, W. Calvin, R. Clancy, K. Edgett, L. Edwards, R. Haberle, P. James, S. Lee, M. Ravine, P. Thomas, and M. Wolff. 2007. Context Camera Investigation on board the Mars Reconnaissance Orbiter. *Journal of Geophysical Research, 112: CiteID E05S04, doi*: 10.1029/2006JE002808.

Malin, M.C., and K.S. Edgett. 2000. Sedimentary rocks of early Mars. *Science, 290*: 927-1938.

McEwen, A.S., E. Eliason, J. Bergstrom, N. Bridges, C. Hansen, W. Delamere, J. Grant, V. Gulick, K. Herkenhoff, L. Keszthelyi, R. Kirk, M. Mellon, S. Squyres, N. Thomas and C. Weitz. 2007. Mars Reconnaissance Orbiter's High Resolution Imaging Science Experiment (HiRISE). *Journal of Geophysical Research, 112, CiteID E05S02, doi*: 10.1029/2005JE002605.

Nedell, S.S., S.W. Squyres, and D.W. Andersen. 1987. Origin and evolution of the layered deposits in the Valles Marineris, Mars. *Icarus, 70*: 409-441.

Okubo, C.H. and A.S. McEwen. 2007. Fracture-controlled paleo-fluid flow in Candor Chasma, Mars. *Science 315, 983; doi*: 10.1126/science.1136855.

Peterson, C. 1981. A secondary origin for the Central Plateau of Hebes Chasma. *12th Lunar and Planetary Science Convention*, Part B, Pergamon Press, New York, 1459-1471.

Racher, H., M. Slingerland, F. Fueten, R. Stesky, P. MacKinnon, E. Hauber, K. Gwinner, T. Zegers. 2009. Structural Analysis of an Interior Layered Deposit in Southern Coprates Chasma, Mars. *40th Lunar and Planetary Science Convention*, Abstract # 1472.

Rossi, A.P., G. Neukum, M. Pondrelli, S. Van Gasselt, T. Zegers, E. Hauber, A. Chicarro, and B. Foing. 2008. Large-scale spring deposits on Mars? *Journal of Geophysical Research, 113(EO), 8016,* doi:10.1029/2007JE003062.

Schultz, R.A. and J. Lin. 2001. Three-dimensional normal faulting models of the Valles Marineris, Mars, and geodynamic implications. *Journal of Geophysical Research. 106 (B8)*: 16549-16566.

Schultz, R.A. 1998. Multiple-process origin of Valles Marineris basins and troughs, Mars. *Planetary Space Science, 46*: 827-834.

Wyrick, D., D. Ferril, A. Morris, D. Sims and N. Franklin. 2005. Quantifying fault networks on Alba Patera, Mars. *36th Lunar and Planetary Science Convention*, Abstract # 2279.

CHAPTER 5 – OVERALL CONCLUSIONS

The opening of the Valles Marineris is attributed the extensive local tectonism. During the formation of the rift valley, the widening associated with the tectonism led to the linkage of the surrounding ancestral basins and the opening of main linear troughs into the current configuration. As a result, the current geological configuration of North and South Coprates Chasma can be attributed to the formation of the Valles Marineris. Northern Coprates Chasma is suggested to have been a small ancestral basin with ILD deposition pre-dating the opening of the Valles Marineris. During the linkage of these basins, the southern portion was removed leaving the northern wall intact in Northern Coprates Chasma. The central ILD found in the north marks the site of the original ancestral basin. Layering in Southern Coprates Chasma was present prior to the opening of the Valles Marineris. Faulting, most likely associated with the opening of the Valles Marineris resulted in the formation of the elongated and triangular edged deposits found in the southern portion of the chasma. The triangular edged mound is suggested to be a large fault block, back rotated from this faulting with only minor tectonism occurring afterwards. The two deposits were suggested to have been a part of a more regionally extensive deposition that were exposed and displaced by faulting. The exact mode of ILD deposition was not determined. Mineralogical data was only available for the northern portion, thus not providing a consistent view of the entire chasma. However, the observations and conclusions do agree well with the overall model for North and South Coprates Chasma. In both locales, the Valles Marineris opening corresponded to the cessation of major deposition and erosion.